Infrared Spectra of Protonated Uracil, Thymine and Cytosine

Jean-Yves Salpin, Sébastien Guillaumont, Jeanine Tortajada, Luke Mac Aleese, Joel Lemaire, Philippe Maître

Infrared spectra of protonated uracil, thymine and cytosine

Jean-Yves Salpin*, Sébastien Guillaumont and Jeanine Tortajada

Laboratoire d'Analyse et de Modélisation pour la Biologie et l'Environnement (LAMBE) Université d'Evry Val d'Esonne – CNRS – Bâtiment Maupertuis – Boulevard François Mitterrand – 91025 EVRY; FRANCE

Luke MacAleese, Joël Lemaire and Philippe Maitre*
Laboratoire de Chimie Physique – Université Paris Sud Orsay – CNRS – 91405 ORSAY; FRANCE

Corresponding authors:

Jean-Yves Salpin
Tel: 33 1 69 47 76 47 Fax: 33 1 69 47 76 55
e-mail : jean-yves.salpin@univ-evry.fr

Philippe Maître
Tel: 33 1 69 15 74 63 Fax: 33 1 69 15 30 53
e-mail : philippe.maitre@lcp.u-psud.fr

Abstract

Gas phase structure of protonated uracil, thymine and cytosine was probed using mid-infrared multiple photon dissociation (IRMPD) spectroscopy performed at CLIO, the Orsay (France) Free Electron Laser facility. Experimental infrared spectra were recorded for ions generated by electrospray ionization, isolated and irradiated in a quadrupole ion trap, and compared to calculated infrared absorption spectra of the different low-lying isomers computed at the B3LYP/6-31++G(d,p) level. For each protonated base, the global energy minimum was found to correspond to an enolic tautomer, whose infrared absorption spectrum was found to match very well with the experimental IRMPD spectrum, with the exception of a very weak IRMPD signal observed at ~1800 cm^{-1} in the case of the three protonated bases. This signal is likely to be the signature of the second energy lying oxo tautomer. We thus conclude that within our experimental conditions, two tautomeric ions are formed and coexist in the quadrupole ion trap.

Keywords : *infrared spectroscopy, multiple photon absorption, photodissociation, protonated nucleobases, mass spectrometry, electrospray ionization.*

1. Introduction

Uracil (**U**), thymine (5-methyl-uracil; **T**) and cytosine (**C**) are pyrimidic bases and constituents of nucleic acids. In the Watson-Crick[1] structure of nucleic acids, uracil and thymine must adopt the dioxo form **U1** and **T1** (also referred to as canonical, see scheme 1) to be in complementary conformation to the normal amino tautomer of the adenine residue, thus generating the base pairs AU or AT. Likewise, cytosine is found in its amino-oxo form (**C1,** scheme 1) in the GC base pair. However, enol forms of U, T and C may also be generated by proton transfer reaction. Because of the probable relationship between the occurrence of these rare enol tautomeric forms and point mutation developing during nucleic acid replication[2-7], the evaluation of the tautomeric behaviour of these three nucleobases is of fundamental importance, and many experimental [4, 8-25] and theoretical [5, 22, 23, 26-47] studies have been carried out on that topic over the last two decades.

An other intense field of research concerns the acido-basic properties of nucleobases. As a matter of fact, the strength of the hydrogen bonds in base pairs is governed by the proton acceptor ability of the carbonyl oxygen atoms and the proton donor ability of the amino groups. Furthermore, protonation of nucleic acid bases play a crucial role in the stabilization of the triplex structures [48] and in mutagenic processes. [49] Consequently, location of both protonation and deprotonation sites of nucleic acid bases contributes to the understanding of chemical processes that occur in DNA in condensed phase.

Mass spectrometry and theoretical calculations are methods of choice to characterize the thermochemistry associated with acido-basic properties of molecules, and they have been logically used to determine the gas phase basicity [40, 45, 50-61] and acidity [40, 45, 54, 55, 62-69] of nucleobases. However, in the particular case of the basicity, given the fact that (i) several neutral tautomeric forms may coexist in the gas phase, and that (ii) these different forms may

be protonated at different nitrogen or oxygen atoms, the protonated species of these nucleobases may correspond to a mixture of several structures (see scheme 1 for the location and label of the various protonation sites discussed in the text). Wolken and Tureček published several years ago a detailed theoretical study about the protonation of the various tautomers of uracil.[57] They demonstrated that the most stable form of protonated uracil is obtained by protonation of the O7 oxygen of the non-canonical oxo-hydroxo tautomer **U2** (scheme 1) and the resulting proton affinity is significantly different from the value computed for the **U1** tautomer. Similarly, a couple of theoretical studies pointed out that two protonated forms of cytosine (oxo and enol) are very close in energy.[53, 58]

It should be emphasized that there is a lack of structural information about the protonated and neutral forms that are actually investigated. The various mass spectrometric methods used so far (equilibrium, kinetic method) cannot discriminate between different possible structures. Provided sufficiently different deprotonation energies, mixtures of protonated forms of nucleobases could also be characterized by the thermokinetic method. [70-72] However, this method is rather long to implement. In a recent study by Yao et al.[73], different protonated forms of 1-methyl-cytosine have been specifically synthetized, thus allowing for their structural characterization by means of tandem mass spectrometry.

Infrared Multiple Photon Dissociation spectroscopy (IRMPD) of mass-selected ions performed with tandem mass spectrometers has recently been shown to be an interesting approach for the structural characterization. This gas-phase ion spectroscopy is often termed “action spectroscopy” since resonant IR absorption cannot be directly probed due to the low ion density. Nevertheless, provided the use of intense infrared sources, ion fragmentation can be induced by a multiple photon absorption process. With this respect, use of free electron lasers (FEL) provides an intense and a wide tunable mid-IR beam. [74, 75] Various tandem mass spectrometers have been exploited for IRMPD spectroscopy experiments either at FELIX or

at CLIO, and several molecular ions produced by electrospray have been studied recently.[76-81]

IR beam provided by these FEL can be tuned in the mid-infrared range allowing for the characterization of the « molecular fingerprint » in the 600-2000 cm^{-1} energy range. Infrared spectra of molecular ions in the 2500-4000 cm^{-1} frequency range can be also recorded using optical parametric oscillator/amplifier (OPO/OPA) lasers. This spectral range is of particular interest for probing the vibrational shifts associated to the NH and OH stretches involved in hydrogen bonds. As compared to IR FEL, these laser sources present a lower intensity. Nevertheless, providing that a weakly bound cluster can be formed between the molecular ion and a rare gas atom (messenger technique)[82], IR photodissociation spectroscopy has successfully been applied using IR OPO/OPA lasers to characterize the structure of a large variety of gas phase molecular ions [83, 84], including ionic water solvated clusters[85] and, recently, water solvated protonated and lithiated amino-acid (valine).[86] Alternatively, IR spectra can be derived from vibrationally resolved electronic spectra, as illustrated by the recent work on protonated triptophan solvated by a controlled number of water molecules.[87, 88]

In this paper, IRMPD spectroscopy of the protonated uracil, thymine and cytosine generated by electrospray ionization and trapped in a quadrupole ion trap is presented. These experiments have been performed at the CLIO, the IR FEL facility in Orsay. Experimental IRMPD spectra are compared to calculated IR absorption spectra of the lowest energy isomers. As discussed above, structures derived from the different protonation sites of the most stable tautomers of neutral pyrimidic bases have been considered (Scheme 1). In the case of uracil and thymine, the four most stable tautomers of U, T (Scheme 1), as established by previous theoretical studies[28, 37, 40], have been considered, while two additional low-lying energy tautomers were also considered for cytosine.[39, 53] Note that in scheme 1, structures of

thymine are deliberately omitted as thymine is the methylated form of uracil (at the C5 position).

<Scheme 1>

2. Experimental and theoretical methods

2.1 Experimental details.

The present IRMPD spectroscopic investigation has been performed using an experimental platform based on a quadrupole ion trap which has been described in details previously.[76] This experimental setup has been recently used to characterize the structure of protonated methyl esters of amino-acids (alycine, alanine, valine, and leucine)[76, 80], of π-complex of cationic benzene-NO[77],and of the σ Meisenheimer complex associated to the aromatic nucleophilic substitution.[79]

Tunable mid-infrared radiation is produced by the Free Electron Laser (FEL) of CLIO (Centre Laser Infrarouge d'Orsay).[75] This laser is based on a 16-48 MeV linear electron accelerator, and bunches of electrons are injected in an undulator, a periodic magnetic field, which is placed in the optical cavity. Using a fixed electron energy, the energy of the emitted photons can be continuously scanned by adjusting the undulator gap. The mean average power was monitored and found to be quite stable (700-800 mW) over the 1000-2000 cm^{-1} energy range scanned using electrons at 45 MeV. The laser wavelength profile was monitored while recording the spectra with a monochromator associated with a pyroelectric detector array (spiricon). The IR-FEL spectral width, which can be adjusted through a tuning of the optical cavity length, was found to be less than 0.5 % of the central wavelength.

Our tandem mass spectrometer is a modified Bruker Esquire 3000 quadrupole ion trap. Multistage mass spectrometry was carried out using the standard Bruker Esquire Control (v5.2) software, and mass-selected ions were irradiated using the MS2 step where the

excitation amplitude was set to 0 to avoid any CID-like process. Mass spectra were recorded after 10 accumulations, using the standard mass range (m/z 50-3000) and the normal scan resolution (13000 Th/s), the accumulation time being typically of 2 ms. This sequence was repeated nine times for each photon energy.

A conical hole (0.7 mm of diameter) in the ring electrode of the trap was made in order to allow the optical access to the center of the trap. The IR-FEL beam is mildly focussed using a 1m focal length spherical mirror, and enters the vacuum chamber through a ZnSe window oriented near to the Brewster angle. The CLIO FEL temporal structure consists of macropulses of 8 μs duration, at a repetition rate of 25 Hz. Each macropulse contains about 500 micropulses each of few picoseconds long. In the present case, it should be noticed that only two trains of pulses were used for irradiating mass-selected ions.[76]

10^{-4} M aqueous solutions of the nucleobases were prepared in pure water (purified with a Milli-Q water purification system) and were introduced in the source using direct infusion with a syringe pump. ESI conditions used were as follows: flow rate of 3 μl/min, spray voltage 3500 V and a capillary temperature of 473 K. Finally, note that temperature of ions in a similar ion trap has been estimated to be 310±10K, using equilibrium constant measurement of ion-molecule complex formation.[89] Phenomenological temperature experienced by the ions in our ion trap should be in this range.

2.2 theoretical calculations.

Molecular orbital DFT calculations were carried out using the B3LYP density functional[90],[91], as implemented in the Gaussian-98 set of programs.[92]

The different protonated forms considered have first been optimized with the 6-31++G(d,p) basis set, without any symmetry constraint. Harmonic vibrational frequencies were estimated at this level to characterize the stationary points as local minima or saddle points, and to

estimate the zero-point vibrational energy (ZPE) corrections. Finally, relative energies were refined using the extended basis set 6-311++G(3df,2p). This high level of calculation is mandatory to correctly estimate the activation barriers associated with the various tautomerization processes considered here. The infrared absorption spectra were calculated within the harmonic approximation. Ghomi et al. [93, 94] have shown in detail that DFT and MP2 levels of theory gave similar results for the geometrical and vibrational features of the nucleic acid base. Furthermore, provided the use of an appropriate scaling factor, hybrid DFT methods such as B3LYP have been shown to outperform other DFT methods as well as traditional *ab initio* approaches to describe both position [95] and relative intensities [96] of IR bands. As far as the positions are concerned, a scaling factor value of 0.96 has been chosen on the basis if the overall good agreement between experimental and computed frequencies for a large set of molecules.[97] Finally, to be consistent with the experimental spectral resolution, the calculated spectra have been convoluted by a 20 cm^{-1} large Lorentzian function.

3. Results, discussion

3.1 Low-energy isomers of protonated U, T and C.

The four most stable protonated forms of uracil and cytosine obtained at the B3LYP/6-311++G(3df,2p)//B3LYP/6-31++G(d,p)+ZPE level of theory, are given in Figure 1. As the relative energy ordering obtained for uracil and thymine are equivalent, protonated forms of thymine have been deliberately omitted. Energetics and structure of all the protonated forms considered in this study are provided in sections 1S and 2S of the supporting information.

Protonation of uracil has been the subject of three recent detailed theoretical studies[40, 57, 98], which concluded that the most stable protonated form of uracil was **U2_ha**, then followed by **U1_hd** (Figure 1), regardless of the method of calculation (B3LYP, MP2 or QCISD(T)). Our study is in agreement with these findings, and points out a small energy difference (+4.2

kJ/mol). As said above, a similar energy order is obtained for thymine (**T2_ha**<**T1_hd**). Nevertheless, it should be noted that the energy difference is slightly larger for thymine (9.0 kJ/mol) than for uracil, which may be due to the steric repulsion between the O8-H hydroxyl and the methyl group located on C5 in **T1_hd**.

It is worth noting that the global minimum **U2_ha** cannot be generated directly from protonation of the dioxo form **U1**, which is, by far, the most stable tautomeric form of neutral uracil in both condensed and gas phase. [28, 30, 35, 37, 40] In the case of protonated cytosine, however, the two lowest energy tautomers, the oxo **C1_hb** and the enol **C1_hc** structures (Figure 1) can be generated by protonation of the most stable neutral tautomer of cytosine.

The enolic tautomer **C1_hc** is predicted to be the global minimum but the oxo **C1_hb** tautomer is only 0.3 kJ/mol higher in energy. This energy ordering is in agreement with both B3LYP/6-31+G(d,p)[98] and MP2 investigations[53, 58]. Note that the opposite energetic order was predicted by an earlier DFT study. [56] As a matter of fact, a recent study of protonated cytosine by Tureček and co-workers demonstrates that use of diffuse functions is essential to accurately evaluate the relative energies between the various protonated forms, and at the highest level of theory considered (CCSD(T)/aug-cc-pVTZ)) **C1_hc** was found to be more stable than **C1_hb** by 7 $kJ.mol^{-1}$.[99] Finally, it should be recalled that the orientation of the hydroxyl group in **C1_hc** is quite important. Indeed, **C1_hc** and **C1_hd** structures only differ by the rotation of 180° of the hydroxyl group but the energy difference between these two forms is rather important. This illustrates the effects of the repulsive interaction between parallel N1-H and O7-H bonds (**C1_hd**) and of the attractive interaction between the O7-H bond and the lone pair of adjacent N3 (**C1_hc**). To complete this survey, it is worth mentioning that all the other hydroxo forms are significantly less stable, while imino species are extremely disfavored (see supporting information).

3.2 IRMPD spectra: overview

On resonance with an infrared active mode of the mass-selected ions, loss of ammonia is observed for the three protonated pyrimidic bases investigated here. For uracil and thymine, loss of isocyanic acid (HNCO) was also detected, but in small amounts. The IRMPD spectra remain unchanged when the two dissociation routes are taken into account. So, we decided to only consider the fragment channel common to the three protonated bases, namely loss of ammonia. The maximum fragmentation yield was about 10% (cytosine, uracil) and 20% (thymine) using only two IR-FEL macropulses. This confirms the high efficiency of the IRMPD process when molecular ions are irradiated in a quadrupole ion trap.[76] IRMPD spectra presented here correspond to the fragmentation efficiency, defined as -ln[Parent/(Parent+Fragments)], as a function of the photon wavenumber.[100]

IRMPD spectra of cytosine, uracil, and thymine are given in Figure 2c, 3c and 4c, respectively. The assignment of the IRMPD spectrum of protonated uracil, thymine and cytosine, is based on their comparison with the spectra computed for the various low energy lying isomers. To make the comparison easier, computed absorption cross-sections are represented in Figures 2-4, assuming a Lorentzian profile (fwhm=20 cm^{-1}) for each calculated infrared band.

As it will be discussed in details later, there is a quite good agreement between the IRMPD spectrum and the calculated IR absorption spectrum of the lowest energy isomer of each protonated pyrimidic base, which corresponds to an enolic form with the exception of one band: a relatively *weak* IRMPD signal observed at about 1800 cm^{-1} for each protonated pyrimidic base. One cannot discard the possibility that the IRMPD band at ~1800 cm^{-1} could be assigned to a combination mode. Indeed, it has been evidenced that an IRMPD signal could be observed when the IR-FEL is on resonance with a combination mode. These conclusions were reached, for example, in the case of proton bound dimer of water[101], and it

was suggested that the combination mode involves the very strongly IR active mode associated to the asymmetric O-H^+-O stretch. It has also been concluded that a combination band involving the very strongly IR active NO stretching mode of the π-complex Bz-NO^+ could lead to an IRMPD signal.[77] In the present case, the calculated IR intensities of the enolic tautomer are much weaker than the two aforementioned cases for which combination modes have been shown to lead to an IRMPD signal. The IRMPD band observed at ~1800 cm^{-1} could rather be the result of a resonant absorption through the very *strongly* infrared active C=O stretch. Nevertheless, considering the strong infrared cross-section associated to the carbonyl group, it is surprising to observe a relatively small IRMPD efficiency on resonance with this vibrational mode.

3.3 IR spectra of protonated cytosine

The experimental IRMPD spectrum of protonated cytosine (Figure 2c) is dominated by a broad band (fwhm~70 cm^{-1}) centered at 1625 cm^{-1}. This band displays an asymmetric profile with a maximum at 1641 cm^{-1} and a shoulder at 1605 cm^{-1}. Three less intense bands were also detected at c.a. 1200, 1502 and 1804 cm^{-1}. Finally, a very weak signal could also be considered around 1440 cm^{-1}. For the sake of clarity, the positions and intensities (km/mol) of only the main IR active vibrational modes of **C1_hb** and **C1_hc** are provided in Table 1.

The C=O stretching mode constitutes an excellent infrared diagnostic of the presence of an oxo form of protonated cytosine in the ion trap. The calculated frequency for the C=O stretching vibration of the **C1_hb** oxo isomer is 1800 cm^{-1}, and the calculated IR spectrum of the lowest energy **C1_hc** enol structure does not display any infrared active mode in this energy range. Therefore, the IRMPD signal observed at 1804 cm^{-1} may suggest that the **C1_hb** oxo isomer is present under our experimental conditions.

On the other hand, the lower energy region of the IRMPD spectrum, and especially the largest IRMPD feature at 1641 cm^{-1}, nicely matches with the calculated IR absorption spectrum of the lowest energy **C1_hc** isomer.

The largest IRMPD feature is observed at 1641 cm^{-1} is quite broad (fwhm~70 cm^{-1}). Indeed, using the same experimental setup, isolated IR active vibrational modes give rise to narrower IRMPD band, with a width of typically 25 cm^{-1} or less.[76] As a result, it is likely that the large IRMPD band observed at 1641 cm^{-1} is the result of the convolution of two or more IRMPD features resulting from the multiple photon absorption through different IR active modes. The experimental IRMPD maximum is observed at 1641 cm^{-1}, only slightly red-shifted as compared to the strongest IR absorption band (1645 cm^{-1}) of structure **C1_hc**. More importantly, the **C1_hc** has two strong absorption bands at 1622 and 1645 cm^{-1}, which could explain the broad character of the IRMPD band observed at 1641 cm^{-1}. Interestingly, one may notice that the shape of the strong IRMPD band centered 1625 cm^{-1}, i.e. the observation of the shoulder on the red-side of the band, could even be explained considering the relative calculated intensities of the infrared absorption bands at 1622 and 1645 cm^{-1} of the enol isomer **C1_hc**. On the contrary, the oxo **C1_hb** tautomer has only one strongly infrared active mode in this energy range (at 1639 cm^{-1}, see Table 1). The selective formation of this oxo isomer should give rise to a narrow IRMPD band around 1600 cm^{-1}.

On the basis of the above discussion, it is likely that both **C1_hc** and **C1_hb** tautomers are simultaneously present under our experimental conditions. Considering the multiple photon character of the IRMPD process, the relative IRMPD band intensities should be taken with caution. Nevertheless, as mentioned above, it is interesting to note that the calculated infrared cross section of the **C1_hb** isomer at 1800 cm^{-1} is almost as large as at 1600 cm^{-1}. As a result, if the **C1_hb** oxo isomer would be selectively formed, one would have expected a stronger IRMPD signal at 1804 cm^{-1}, i.e. of the same order of magnitude as the one observed at ~1600

cm^{-1}. The shape of the IRMPD spectrum could therefore result from the superposition of a minor contribution of the oxo isomer (**C1_hb**) and a major contribution of the lowest energy structure, an enolic isomer (**C1_hc**). A dominant enolic form is consistent with the calculated relative energies of these two competing structures. The formation of the enolic **C1_hc** tautomer of protonated cytosine was also proposed recently, based on the measured enthalpy and entropy associated to the cluster formation between protonated cytosine and ammonia.[98] An assignment of the IRMPD band can be made on the basis of the analysis of the infrared active modes of **C1_hb** and **C1_hc** given in Table 1. Overall, there is a quite good agreement between the IRMPD spectrum (Figure 2c) and the calculated IR absorption spectrum of **C1_hc** (Figure 2b) which we assume to be the most abundant species in the ion trap. The strongest IRMPD band centered at 1625 cm^{-1} could be assigned to the contribution of three IR active modes of the lowest energy **C1_hc** isomer. The calculated infrared absorption spectrum of this structure displays two strongly active IR modes corresponding to the C2-O7 stretch (1584 cm^{-1}) and a coupling of the C5-C6 and C2-N3 stretches (1645 cm^{-1}), but also a relatively strong absorption feature at 1622 cm^{-1} associated to the NH_2 scissoring. As said above, it is likely that the fragmentation of the oxo **C1_hb** isomer, which has a strongly infrared active band at 1639 cm^{-1} (see Table 1), also contributes to the large and broad IRMPD band centered at 1625 cm^{-1}. Similarly, the two small IRMPD bands observed at 1200 and 1502 cm^{-1} nicely match with the IR absorption bands of the lowest energy **C1_hc** isomer, but it is likely that on resonance infrared multiple photon absorption could occur with the oxo **C1_hb** isomer, which has two strong absorption bands at 1204 and 1515 cm^{-1} (Table 1).

3.4 IR spectra of protonated uracil and thymine

The computed IR spectra of the two most stable forms of protonated uracil and thymine, are presented in Figure 3 and 4, respectively, while the position and intensity

(km/mol) of the main bands are summarized in Table 2 and 3. As expected, the IRMPD spectra of protonated uracil and thymine share several common features (Figures 3c and 4c). The only difference between the two spectra is due to the presence of the methyl group of thymine characterized by an IR absorption at ~1400 cm^{-1}, which probably explains why the IRMPD signal at ~1400 cm^{-1} is enhanced in thymine as compared to uracil. The two IRMPD spectra are dominated by a strong IRMPD band at ~1600 cm^{-1}, a broad signal between 1150 and 1250 cm^{-1}, and a small feature around 1300-1320 cm^{-1}.

Overall, for both uracil and thymine protonated systems, there is a quite good agreement between the IRMPD spectrum and the calculated infrared absorption spectrum of the lowest energy isomer (see Figures 3-4), and the analysis of the 1300-1700 cm^{-1} energy region provides evidence that the enol tautomer contributes mostly to the IRMPD spectrum. The first evidence is associated to the IRMPD signal in the 1300-1350 cm^{-1} range. This is particularly true for protonated thymine, the IRMPD band at 1368 cm^{-1} being in very good agreement with the infrared active band at 1355 cm^{-1} of the enol isomer **T2_ha**. In the case of protonated uracil, the IRMPD band at 1316 cm^{-1} can be also considered as a signature of the enol form **U2_ha**, whose IR absorption spectrum displays a strong IR band at 1349 cm^{-1}. For both ions, the IRMPD band observed in the 1300-1350 cm^{-1} can be assigned to a δ CNH mode of the enolic form. On the contrary, the higher energy oxo tautomer of protonated uracil or thymine does not display any significant infrared band between 1300 and 1350 cm^{-1}.

The shape of the IRMPD spectra between 1400 and 1650 cm^{-1} is also in good agreement with the infrared cross section of the corresponding enol isomers, assuming that each calculated IR band has a lorentzian profile (fwhm=20 cm^{-1}). In the case of protonated uracil, the IRMPD band at 1469 cm^{-1} is observed slightly red-shifted from the calculated position (1487 cm^{-1}) of the ν-C4-O8 stretch of **U2_ha**. The IRMPD band centered at 1589 cm^{-1} is in good agreement with the sum of the contributions of two strongly infrared active modes of **U2_ha** calculated

at 1602 and 1630 cm^{-1}, and corresponding to the coupling of ν_{CC} with ν_{CO} and ν_{CN}, respectively (Table 2). It is interesting to note that the IRMPD bandwidth (fwhm=45 cm^{-1}) clearly suggests that the IRMPD band at 1589 cm^{-1} is the result of the absorption through two closely spaced IR active modes, as it is the case for the calculated IR absorption spectrum of **U2_ha**. On the other hand, our calculations suggest that the oxo isomer **U1_hd** has two well separated strongly IR active bands (1558 and 1606 cm^{-1}, see Table 2). Furthermore, the infrared cross section of the oxo form **U1_hd** is quite significant and does not vanish between 1400 and 1650 cm^{-1}, and our calculations even predict that **U1_hd** has a strong IR band at 1558 cm^{-1} associated with the ν-C4-C5 (Table 2), whereas the IRMPD signal vanishes at about this photon energy (Figure 3).

The 1400-1650 cm^{-1} region of the IRMPD spectrum of protonated thymine is also in good agreement with the infrared cross section of the enolic form **T2_ha** (Figure 4), which displays two absorption bands in this region. On the contrary, the oxo form **T1_hd** has a strong absorption band at 1538 cm^{-1}, whereas no IRMPD signal is detected at this photon energy. The observation of a signal at 1474 cm^{-1} can be considered as characteristic of the **T2_ha** structure. This band may indeed correspond to the IR absorption band calculated at 1472 cm^{-1}, which is associated to a normal mode resulting from the coupling of the ν-C4-O8 and of the δ-CH_3 bending vibrations. The strongest IRMPD signal is observed on resonance with the maximum of the calculated infrared cross section of **T2_ha**. Two strongly infrared active bands contribute to the infrared cross section: the IR absorption bands at 1599 and 1628 cm^{-1} correspond to the coupling of ν_{CC} with ν_{CO} and ν_{CN} respectively (Table 3).

The broad IRMPD feature observed in the 1100-1250 cm^{-1} region for both protonated uracil and thymine also reproduces the shape of the infrared cross-section of the enolic form. In both cases, the analysis of the normal modes reveals that they result from the coupling of δ_{COH}, δ_{COH} and δ_{CNH} local modes.

Finally, as in the case of protonated cytosine, an IRMPD signal is observed at ~1800 cm^{-1} for both protonated uracil and thymine. This band may suggest that the oxo tautomer (**U1_hd** and **T1_hd** for uracil and thymine, respectively) are also present under our experimental conditions. Note that the calculated infrared intensity associated to the CO stretch at ~1800 cm^{-1} is very large for these structures. Consequently, even if rigorous quantitation cannot be made, one may deduce from our experiments that the enol forms **U2_ha** and **T2_ha**, which are predicted to be the lowest energy structure for both protonated uracil and thymine, are the most abundant species formed under our experimental conditions.

3.5 Discussion

Our results suggest that under our experimental conditions, protonated cytosine, uracil and thymine exist as a mixture of two different structures: an oxo form that should be present as a minor fraction, and a dominant species corresponding to an enol form and predicted to be the lowest energy structure. These findings deserve a discussion since the enol forms cannot always arise from a direct protonation of the most stable tautomer of the bases.

In the case of protonated uracil and thymine, IRMPD data strongly suggest that the lowest energy enol tautomer is the most abundant species formed under our experimental conditions. This is in contrast with gas phase studies related to the determination of the proton affinity of these two nucleobases. It has indeed been shown that, for example, the measured proton affinity of uracil should correspond to the protonation of the most stable tautomer (**U1**), leading to the formation of **U1_hd**.[57] Whereas the enol form **U2_ha** is more stable, the calculated proton affinity associated with this tautomer would be too high as compared to the experimental value.[57] Most importantly, it should be recalled that neutral uracil and thymine only present one low energy lying isomer (**U1** and **T1** respectively) in both condensed and gas phase, and that the enolic form (**U2_ha** and **T2_ha**, respectively) could not be generated

directly under single collision conditions through a proton transfer from a protonating agent to this tautomer. Note that data about protonated forms of uracil and thymine in solution are rather scarce. However, several reports seem to conclude that protonation of the three pyrimidic bases in solution should occur preferentially at N3 (scheme 1), [102-105] leading in the particular case of U and T to the forms called **U1_hf** and **T1_hf** (see supporting information). Though minima in the gas phase, these forms are quite unstable and are not observed experimentally, their IR spectra (two strong absorptions at 1827 and 1867 cm^{-1}, $\nu_{C=O}$) being radically different from the experimental spectrum.

Consequently, tautomerization of either neutral or protonated uracil and thymine must be envisaged in order to account for the formation of enol tautomer of the protonated species. Tautomerization of the isolated neutral species is energy demanding. For instance, the **U1** → **U2** tautomerisation presents an activation barrier located 168.4 $kJ.mol^{-1}$ above **U1**. Nevertheless, this process could probably be significantly facilitated by protic solvent molecule(s). The most stable structure of uracil-water cluster corresponds to a structure where the water molecule forms a bridge between O4 and N3(H) of **U1**. [41, 44] This configuration is favourable for a potential water-catalyzed double proton transfer between **U1** and **U2**. The corresponding transition state is hexahydric, water acting as a bridge. The formation of this six-membered ring lowers the activation energy considerably (-101.3 $kJ.mol^{-1}$). Furthermore, Hu et al have shown that adding a second molecule of water in the N3-O4 region further decreases the activation barrier for tautomerization.[44] It is thus conceivable that water solvent molecules in solution or within the electrospray droplets may assist in the tautomerizing of **U1**/**U2** prior to protonation.

Tautomerization of protonated species may also be envisaged. Gas-phase **U1_hd→U2_ha** interconversion has been studied. This reaction can be viewed as a two-step process (see section 3S of the supporting information). The rate-limiting step (the 1,3 proton transfer) is

associated with an activation barrier of 169 kJ.mol^{-1}. At thermal energies, such a process is precluded. The same result is found for protonated thymine (see section 5S of the supporting information). So, the two protonated forms are present in the gas phase prior to the IRMPD event and **U2_ha** (**T2_ha**) cannot be formed from **U1_hd** (**T1_hd**) via this pathway. Similar results were recently obtained by Wu and McMahon. On the other hand, these authors showed that tautomerization of protonated uracil and thymine can be significantly favoured by a protic solvent. Wu and McMahon indeed studied the energetics associated to the cluster formation between ammonia and protonated nucleic acid bases, including cytosine, uracil, and thymine. High pressure mass spectrometry was used, and the measured enthalpy and entropy were compared to the ones obtained at the MP2(full)/6-311++G(2d,2p)//B3LYP/6-31+G(d,p) level of theory. In the case of thymine, for example, the best agreement between experimental and theoretical results was obtained when considering that the dominant species participating to the equilibrium are NH_3 and **T2_ha**, leading to the lowest energy structure of the cluster where a hydrogen bond is formed between an enol group and the nitrogen of ammonia. Since this interpretation relies on the existence of the enol tautomer **T2_ha** of thymine in the gas phase, Wu and McMahon investigated the **T1_hd→T2_ha** tautomerization reaction. While the calculated energy barrier at their highest level of theory is quite high (170 kJ/mol), as found in the present study (171 kJ/mol), for the isolated protonated thymine, Hu and McMahon showed that this tautomerization becomes facile at thermal energies through a bimolecular association with a protic molecule such as ammonia.[98] Ammonia then acts as a proton carrier, resulting in a transition state associated with the 1,3 proton shift lying much lower in energy than the reactants and products. Consequently, one can reasonably assume that in a protic solvent such as water, solvent molecules may also assist in a similar fashion both **T1_hd→T2_ha** and **U1_hd→U2_ha** interconversions during their transfer in the gas-phase by electrospray like in the present experimental conditions.

Concerning cytosine, both the lowest energy enol tautomer **C1_hc** and the slightly higher energy oxo one **C1_hb** can be generated by gas-phase protonation of the canonical form **C1**. **C1_hc** may also arise from hydroxo tautomers as both experimental[14, 18, 20], and theoretical[30, 31, 34, 39, 43, 53, 58] studies suggest that cytosine might exist in the gas phase as a mixture of **C1**, and the two enol-amino tautomers **C2** and **C3**. Accordingly, **C1_hc** could be generated directly from **C2** by protonation at N1 (the most basic site of **C2**). Protonation of **C3** directly leads to **C1_hd** and a subsequent 180° rotation of the OH group is required to generate **C1_hc**. Such rotation may occur quite easily, because it is associated with a very small activation barrier: at our highest level of calculation, the corresponding transition state lies 10.2 kJ/mol above **C1_hd** (see sections 6S and 7S of the supporting information). On the other hand, the isomerization barrier between the two lowest energy of protonated cytosine is very high. The transition state associated to the **C1_hb** → **C1_hc** isomerization through a 1,3 proton shift has an activation barrier of 159 kJ.mol^{-1}. This strongly suggests that the two protonated forms which are shown to coexist in the ion trap under our experimental conditions, do not interconvert in the gas phase.

It is also likely that tautomer **C1** may be protonated in solution. As a matter of fact, several experimental and theoretical reports have indeed indicated that **C1** is the preferred tautomer in solution.[8, 36, 39, 53] and that protonation occurs at N3 site [102, 104, 105], with a pK value of 4.7[103], not far from the pH of our solution (5). Consequently, protonation in solution would lead to the **C1_hb** form and therefore tautomerization has to take place to account for the major structure observed experimentally (**C1_hc**). Like for uracil and thymine, isomerization of the protonated form **C1_hb**, assisted by a protic solvent molecules, may also be envisaged. Isomerization in solution might also precede protonation and involve the various neutral forms. Gorb et al.[36] found that the height of proton-transfer barrier associated with the **C1** → **C3** isomerization for monohydrated cytosine complexes (58.2 kJ.mol^{-1}; water-catalysed

double proton transfer process between N1 and O7 sites), is approximately three times lower than for isolated systems. Our calculations lead to the same conclusion.

Conclusion

The structure of gaseous protonated uracil, thymine and cytosine was probed using mid-infrared multiple photon dissociation (IRMPD) spectroscopy. Overall, for the three protonated species, there is a good agreement between experimental IRMPD spectrum recorded between 1000 and 2000 cm^{-1} and the calculated infrared absorption spectrum of the lowest energy lying tautomer (enol form). A fraction of the second most stable form (oxo tautomer) is also evidenced by the presence of a IRMPD signal at ~1800 cm^{-1}. Nevertheless, this signal is small. Furthermore, in the case of protonated thymine and uracil in particular, no IRMPD signal was observed on resonance with other infrared active modes of the oxo isomer. We thus conclude that the most abundant tautomer generated under our experimental conditions corresponds to the enol structure, which has long been recognized as the lowest energy tautomer.[40, 57, 98] In order to account for our spectroscopic observation of the enol isomers as most abundant species, it is proposed that tautomerization of either neutral or protonated nucleobases should be relatively facile in a protic solvent, prior to or during their transfer into the gas phase by the electrospray process.

Acknowledgements

The authors would like to thank the Institut du Développement et des Ressources en Informatique Scientifique (IDRIS, CNRS) for computational time. Generous financial support

by the European Commission through the NEST/ADVENTURE program (EPITOPES, project #15637) is also gratefully acknowledged (J.L. and P.M.). We thank Jean-Michel Ortega and the CLIO team for their support during the experiments.

Supporting information

Structures, energetics and potential energy surfaces associated with tautomerization of protonated uracil, thymine and cytosine, are provided as a supporting information.

Bibliography

[1] J. D. Watson, F. H. Crick *Nature*. **1953**, *171*, 964-967.

[2] P. O. Lowdin *Rev. Mod. Phys.* **1963**, *35*, 724-732.

[3] M. D. Topal, J. R. Fresco *Nature*. **1976**, *263*, 285-289.

[4] L. C. Sowers, G. V. Fazakerley, R. Eritja, B. E. Kaplan, M. F. Goodman *Proc. Nat. Acad. Science USA*. **1986**, *83*, 5434-5438.

[5] J. Florian, J. Leszczynski *J. Am. Chem. Soc.* **1996**, *118*, 3010-3017.

[6] E. S. Kryachko *Int. J. Quantum Chem.* **2002**, *90*, 910-923.

[7] E. S. Kryachko, J. R. Sabin *Int. J. Quantum Chem.* **2003**, *91*, 695-710.

[8] M. Dreyfus, O. Bensaude, G. Dodin, J. E. Dubois *J. Am. Chem. Soc.* **1976**, *98*, 6338-6349.

[9] P. Beak *Acc. Chem. Res.* **1977**, *10*, 186-192.

[10] H. Ruterjans, E. Kaun, W. E. Hull, H. H. Limbach *Nucleic Acids Res.* **1982**, *10*, 7027-7039.

[11] M. Szczesniak, M. J. Nowak, H. Rostkowska, K. Szczepaniak, W. B. Person, D. Shugar *J. Am. Chem. Soc.* **1983**, *105*, 5969-5976.

[12] D. Dougherty, K. Wittel, J. Meeks, S. P. McGlynn *J. Am. Chem. Soc.* **1984**, *98*, 3815-3820.

[13] S. Chin, I. Scott, K. Szczepaniak, W. B. Person *J. Am. Chem. Soc.* **1984**, *106*, 3415-3422.

[14] E. D. Radchenko, G. G. Sheina, N. A. Smorygo, Y. P. Blagoi *J. Mol. Struct.* **1984**, *116*, 387-396.

[15] M. Fujii, T. Tamura, N. Mikami, M. Ito *Chem. Phys. Lett.* **1986**, *126*, 583-587.

[16] Y. Tsuchiya, T. Tamura, M. Fujii, M. Ito *J. Phys. Chem.* **1988**, *92*, 1760-1765.

[17] B. B. Brady, L. A. Peteanu, D. H. Levy *Chem. Phys. Lett.* **1988**, *147*, 538-543.

[18] M. Szczesniak, K. Szczepaniak, J. S. Kwiatkowski, K. Kubulat, W. B. Person *J. Am. Chem. Soc.* **1988**, *110*, 8319-8330.

[19] R. D. Brown, P. D. Godfrey, D. McNaughton, A. P. Pierlot *J. Am. Chem. Soc.* **1989**, *111*, 2308-2310.

[20] M. J. Nowak, L. Lapinski, J. Fulara *Spectrochim. Acta, Part A.* **1989**, *45*, 229-242.

[21] A. Jaworski, M. Szczesniak, K. Szczepaniak, K. Kubulat, W. B. Person *J. Mol. Struct.* **1990**, *223*, 63-92.

[22] J. Smets, L. Adamowicz, G. Maes *J. Phys. Chem.* **1995**, *99*, 6387-6400.

[23] J. S. Kwiatkowski, J. Leszczynski *J. Phys. Chem.* **1996**, *100*, 941-953.

[24] M. Kubota, T. Kobayashi *J. Electron Spectrosc. Relat. Phen.* **1996**, *82*, 61-70.

[25] Z. Zwierzchowska, K. DobroszTeperek, W. Lewandowski, R. Kolos, K. Bajdor, J. C. Dobrowolski, A. P. Mazurek *J. Mol. Struct.* **1997**, *410*, 415-420.

[26] I. R. Gould, I. H. Hillier *Chem. Phys. Lett.* **1989**, *161*, 185-187.

[27] I. R. Gould, M. A. Vincent, I. H. Hillier, L. Lapinski, M. J. Nowak *Spectrochim. Acta, Part A.* **1992**, *48*, 811-818.

[28] J. Leszczynski *J. Phys. Chem.* **1992**, *96*, 1649-1653.

[29] I. R. Gould, D. V. S. Green, P. Young, I. H. Hillier *J. Org. Chem.* **1992**, *57*, 4434-4437.

[30] D. A. Estrin, L. Paglieri, G. Corongiu *J. Phys. Chem.* **1994**, *98*, 5653-5660.

[31] I. R. Gould, N. A. Burton, R. J. Hall, I. H. Hillier *J. Mol. Struct. Theochem*. **1995**, *331*, 147-154.

[32] G. Paglieri, G. Corongiu, D. A. Estrin *Int. J. Quantum Chem.* **1995**, *56*, 615-625.

[33] J. Leszczynski, J. Sponer *J. Mol. Struct. Theochem*. **1996**, *388*, 237-243.

[34] S. Morpurgo, M. Bossa, G. O. Morpurgo *Chem. Phys. Lett.* **1997**, *280*, 233-238.

[35] M. Orozco, B. Hernandez, F. J. Luque *J. Phys. Chem. B.* **1998**, *102*, 5228-5233.

[36] L. Gorb, J. Leszczynski *Int. J. Quantum Chem.* **1998**, *70*, 855-862.

[37] S. X. Tian, C. F. Zhang, Z. J. Zhang, X. J. Chen, K. Z. Xu *Chem. Phys.* **1999**, *242*, 217-225.

[38] P. U. Civcir *J. Mol. Struct. Theochem*. **2000**, *532*, 157-169.

[39] C. Aleman *Chem. Phys.* **2000**, *253*, 13-19.

[40] E. S. Kryachko, M. T. Nguyen, T. Zeegers-Huyskens *J. Phys. Chem. A.* **2001**, *105*, 1288-1295.

[41] E. S. Kryachko, M. T. Nguyen, T. Zeegers-Huyskens *J. Phys. Chem. A.* **2001**, *105*, 1934-1943.

[42] M. Rueda, F. J. Luque, J. M. Lopez, M. Orozco *J. Phys. Chem. A.* **2001**, *105*, 6575-6580.

[43] M. Piacenza, S. Grimme *J. Comput. Chem.* **2004**, *25*, 83-98.

[44] X. Hu, H. Li, W. Liang, S. Shijun Han *J. Phys. Chem. B.* **2004**, *108*, 12999-12307.

[45] A. K. Chandra, D. Michalska, R. Wysokinsky, T. Zeegers-Huyskens *J. Phys. Chem. A.* **2004**, *108*, 9593-9600.

[46] S. Millefiori, A. Alparone *Chem. Phys.* **2004**, *303*, 27-36.

[47] X. Hu, H. Li, W. Liang, S. Han *J. Phys. Chem. B.* **2005**, *109*, 5935 - 5944.

[48] M. D. Frankkamenetskii, S. M. Mirkin *Annual Rev. Biochem.* **1995**, *64*, 65-95.

[49] R. R. Sinden, DNA Structure and Function, Academic Press, San Diego CA, **1994**.

[50] M. S. Wilson, J. A. McCloskey *J. Am. Chem. Soc.* **1975**, *97*, 3436-3444.

[51] M. Meotner *J. Am. Chem. Soc.* **1979**, *101*, 2396-2403.

[52] F. Greco, A. Liguori, G. Sindona, N. Uccella *J. Am. Chem. Soc.* **1990**, *112*, 9092-9096.

[53] C. Colominas, F. J. Luque, M. Orozco *J. Am. Chem. Soc.* **1996**, *118*, 6811-6821.

[54] M. T. Nguyen, A. K. Chandra, T. Zeegers-Huyskens *J. Chem. Soc. Faraday Trans.* **1998**, *94*, 1277-1280.

[55] A. K. Chandra, M. T. Nguyen, T. Zeegers-Huyskens *J. Phys. Chem. A.* **1998**, *102*, 6010-6016.

[56] N. Russo, M. Toscano, A. Grand, F. Jolibois *J. Comput. Chem.* **1998**, *19*, 989-1000.

[57] J. K. Wolken, F. Turecek *J. Am. Soc. Mass Spectrom.* **2000**, *11*, 1065-1071.

[58] Y. Podolyan, L. Gorb, J. Leszczynski *J. Phys. Chem. A.* **2000**, *104*, 7346-7352.

[59] M. A. Kurinovich, L. M. Phillips, S. Sharma, J. K. Lee *Chem. Commun.* **2002**, 2354-2355.

[60] L. Di Donna, A. Napoli, G. Sindona, C. Athanassopoulos *J. Am. Soc. Mass Spectrom.* **2004**, *15*, 1080-1086.

[61] S. Mezzache, S. Alves, C. Pepe, M. Quelquejeu, F. Fournier, J. M. Valery, J. C. Tabet *J. Mass Spectrom.* **2005**, *40*, 722-730.

[62] A. K. Chandra, M. T. Nguyen, T. Zeegers Huyskens *J. Mol. Struct.* **2000**, *519*, 1-11.

[63] M. A. Kurinovich, J. K. Lee *J. Am. Chem. Soc.* **2000**, *122*, 6258-6262.

[64] E. C. M. Chen, E. S. Chen *J. Phys. Chem. B.* **2000**, *104*, 7835-7844.

[65] S. Gronert, W. Y. Feng, F. Chew, W. M. Wu *Int. J. Mass Spectrom.* **2000**, *196*, 251-258.

[66] M. A. Kurinovich, J. K. Lee *J. Am. Soc. Mass Spectrom.* **2002**, *13*, 985-995.

[67] H. Moustafa, S. El-Taher, M. F. Shibl, R. Hilal *Int. J. Quantum Chem.* **2002**, *87*, 378-388.

[68] A. K. Chandra, T. Uchimaru, T. Zeegers-Huyskens *J. Mol. Struct.* **2002**, *605*, 213-220.

[69] T. M. Miller, S. T. Arnold, A. A. Viggiano, A. E. S. Miller *J. Phys. Chem. A.* **2004**, *108*, 3439-3446.

[70] G. Bouchoux, J. Y. Salpin, D. Leblanc *Int. J. Mass Spectrom.* **1996**, *153*, 37-48.

[71] G. Bouchoux, M. T. Nguyen, J. Y. Salpin *J. Phys. Chem. A.* **2000**, *104*, 5778-5786.

[72] M. Mormann, J. Y. Salpin, D. Kuck *Int. J. Mass Spectrom.* **2006**, *249*, 340-352.

[73] C. X. Yao, M. L. Cuadrado-Peinado, M. Polasek, F. Turecek *J. Mass Spectrom.* **2005**, *40*, 1417-1428.

[74] D. Oepts, A. F. G. Van der Meer, P. W. Van Amersfoort *Infrared Phys. Technol.* **1995**, *36*, 297-308.

[75] R. Prazeres, F. Glotin, C. Insa, D. A. Jaroszynski, J. M. Ortega *Eur. Phys. J. D.* **1998**, *3*, 87-93.

[76] L. MacAleese, A. Simon, T. B. McMahon, J. M. Ortega, D. Scuderi, J. Lemaire, P. Maitre *Int. J. Mass Spectrom.* **2006**, *249*, 14-20.

[77] B. Chiavarino, M. E. Crestoni, S. Fornarini, J. Lemaire, P. Maitre, L. MacAleese *J. Am. Chem. Soc.* **2006**, *128*, 12553-12561.

[78] N. C. Polfer, J. Oomens, D. T. Moore, G. von Helden, G. Meijer, R. C. Dunbar *J. Am. Chem. Soc.* **2006**, *128*, 517-525.

[79] B. Chiavarino, M. E. Crestoni, S. Fornarini, F. lanucara, J. Lemaire, P. Maitre *Angew. Chem.* **2007**, *In press*.

[80] A. Simon, L. MacAleese, P. Maitre, J. Lemaire, T. B. McMahon *J. Am. Chem. Soc*. **2007**, *129*.

[81] G. S. Groenewold, A. K. Gianotto, K. C. Cossel, M. J. Van Stipdonk, J. Oomens, N. Polfer, D. T. Moore, W. A. de Jong, M. E. McIlwain *PhysChemChemPhys*. **2007**, *9*, 596-606.

[82] M. Okumura, L. I. Yeh, Y. T. Lee *J. Chem. Phys.* **1985**, *83*, 3705-3706.

[83] K. R. Asmis, G. Santambrogio, M. Brummer, J. Sauer *Angew. Chem., Int. Ed. Engl.* **2005**, *44*, 3122-3125.

[84] O. Dopfer *J. Phys. Org. Chem.* **2006**, *19*, 540-551.

[85] J. M. Headrick, E. G. Diken, R. S. Walters, N. I. Hammer, R. A. Christie, J. Cui, E. M. Myshakin, M. A. Duncan, M. A. Johnson, K. D. Jordan *Science*. **2005**, *308*, 1765-1769.

[86] A. Kamariotis, O. V. Boyarkin, S. R. Mercier, R. D. Beck, M. F. Bush, E. R. Williams, T. R. Rizzo *J. Am. Chem. Soc.* **2006**, *128*, 905-916.

[87] O. V. Boyarkin, S. R. Mercier, A. Kamariotis, T. R. Rizzo *J. Am. Chem. Soc.* **2006**, *128*, 2816-2817.

[88] S. R. Mercier, O. V. Boyarkin, A. Kamariotis, M. Guglielmi, I. Tavernelli, M. Cascella, U. Rothlisberger, T. R. Rizzo *J. Am. Chem. Soc.* **2006**, *128*, 16938-16943.

[89] S. Gronert *J. Am. Soc. Mass Spectrom.* **1998**, *9*, 845.

[90] C. Lee, W. Yang, R. Parr *Phys. Rev. B: Condens. Matter*. **1988**, *37*, 785-789.

[91] A. D. Becke *J. Chem. Phys.* **1993**, *98*, 5648-5652.

[92] M. J. Frisch, G. W. Trucks, H. B. Schlegel, G. E. Scuseria, M. A. Robb, J. R. Cheeseman, V. G. Zakrzewski, J. A. Montgomery Jr, R. E. Stratmann, J. C. Burant, S. Dapprich, J. M. Millam, A. D. Daniels, K. N. Kudin, M. C. Strain, O. Farkas, J. Tomasi, V. Barone, M. Cossi, R. Cammi, B. Mennucci, C. Pomelli, C. Adamo, S. Clifford, J. Ochterski, G. A. Petersson, P. Y. Ayala, Q. Cui, K. Morokuma, D. K. Malick, A. D. Rabuck, K. Raghavachari, J. B. Foresman, J. Ciolowski, J. V. Ortiz, A. G. Baboul, B. B. Stefanov, G. Liu, A. Liashenko, P. Piskorz, I. Komaromi, R. Gomperts, R. L. Martin, D. J. Fox, T. Keith, M. A. Al-Laham, C. Y. Peng, A. Nanayakkara, C. Gonzalez, M. Challacombe, P. M. W. Gill, B. Johnson, W. S. Chen, M. W. Wong, J. L. Andres, M. Head-Gordon, E. S. Replogle, J. A. Pople in Gaussian 98, Revision A.7, Vol. (Ed.^Eds.: Editor), Gaussian Inc., Pittsburgh PA, 1998., City.

[93] M. P. Gaigeot, N. Leulliot, M. Ghomi, H. Jobic, C. Coulombeau, O. Bouloussa *Chem. Phys.* **2000**, *261*, 217-237.

[94] A. Hocquet, N. Leulliot, M. Ghomi *J. Phys. Chem. B.* **2000**, *104*, 4560-4568.

[95] M. D. Halls, J. Velkovski, H. B. Schlegel *Theor. Chem. Acc.* **2001**, *105*, 413-421.

[96] M. D. Halls, H. B. Schlegel *J. Chem. Phys.* **1998**, *109*, 10587-10593.

[97] in NIST Computational Chemistry Comparison and Benchmark Database. NIST Standard Reference Database Number 101., Vol. (Ed.^Eds.: Editor), Russell D. Johnson III, City, **2005**.

[98] R. Wu, T. B. McMahon *J. Am. Chem. Soc.* **2007**, *129*, 569-580.

[99] C. Yao, F. Tureček, M. J. Polce, C. Wesdemiotis *Int. J. Mass Spectrom.* **2007**, *265*, 106-123.

[100] J. Lemaire, P. Boissel, M. Heninger, G. Mauclaire, G. Bellec, H. Mestdagh, A. Simon, S. Le Caer, J. M. Ortega, F. Glotin, P. Maitre *Phys. Rev. Lett.* **2002**, *89*, 273002-273001.

[101] T. D. Fridgen, T. B. McMahon, L. MacAleese, J. Lemaire, P. Maitre *J. Phys. Chem. A.* **2004**, *108*, 9008-9010.

[102] O. Jardetzky, P. Pappas, N. G. Wade *J. Am. Chem. Soc.* **1963**, *85*, 1657-1658.

[103] J. J. Christensen, J. H. Rytting, R. M. Izatt *J. Phys. Chem.* **1967**, *71*, 2700-2705.

[104] R. M. Izatt, J. J. Christensen, J. H. Rytting *Chem. Rev.* **1971**, *71*, 439-481.

[105] S. Ganguly, K. K. Kundu *Can. J. Chem.* **1994**, *72*, 1120-1126.

Table and Figure caption

Table 1: Measured (left column) and calculated vibrational spectra for protonated cytosine. Normalized intensities of the experimental signal are given in parenthesis.

Table 2: Measured (left column) and calculated vibrational spectra for protonated uracil. Normalized intensities of the experimental signal are given in parenthesis.

Table 3 : Measured (left column) and calculated vibrational spectra for protonated thymine. Normalized intensities of the experimental signal are given in parenthesis.

Figure 1: Structure and B3LYP/6-311++G(3df,2P)//B3LYP/6-31+G(d,p)+ZPE relative energies (kJ/mol) of the lowest energy structures obtained of protonated uracil and cytosine. See section 2S of the supporting information for a complete survey of the various structures considered.

Figure 2: IR spectrum of protonated cytosine. DFT calculated IR absorption spectrum of the two lowest isomers **C1_hb (a)** and **C1_hc (b)** compared to the experimental IRMPD spectrum **(c)** recorded with two IR-FEL macropulses with our quadrupole ion trap device.

Figure 3: IR spectrum of protonated uracil. DFT calculated IR absorption spectrum of the two lowest isomers **U1_hd (a)** and **U2_ha (b)** compared to the experimental IRMPD spectrum **(c)** recorded with two IR-FEL macropulses with our quadrupole ion trap device.

Figure 4: IR spectrum of protonated thymine. DFT calculated IR absorption spectrum of the two lowest isomers **T1_hd (a)** and **T2_ha (b)** compared to the experimental IRMPD spectrum **(c)** recorded with two IR-FEL macropulses with our quadrupole ion trap device.

Table 1 : Measured (left column) and calculated vibrational spectra for protonated cytosine. Normalized intensities of the experimental signal are given in parenthesis.

Wavenumber		Calculated intensities ($km.mol^{-1}$)		Vibrational mode
Experimental	Calculated [a]	C1_hb	C1_hc	
1200 (0.15)	1173		223	Combined δ CNH/δ COH/δ CCH modes
	1204	91		Combined δ COH/δ CCH modes
1502 (0.10)	1487		125	ν C4-N8
	1500		40	Combined δ CNH/δ COH/ ν N3-C4 modes
	1515	150		δ CNH + ν N3-C4
1605 (0.71)	1584		482	ν C2-O7
	1603	62		δ NH_2 sc
1641 (1.00)	1622		135	δ NH_2 sc
	1639	787		ν C4-N8
	1645		738	ν C5-C6 + ν C2-N3
1804 (0.03)	1799	679		ν C2=O7

[a] scaled by a 0.96 scaling factor.

Table 2: Measured (left column) and calculated vibrational spectra for protonated uracil. Normalized intensities of the experimental signal are given in parenthesis.

Wavenumber		Calculated intensities (km/mol)		Vibrational mode
Experimental	Calculated [a]	U1_hd	U2_ha	
1138 (0.29)	1125	91		δ COH or combined δ COH/δ CCH modes
	1133		107	
	1142	49		
1174 (0.13)	1169		262	Combined δ CNH/δ COH/δ CCH modes
	1204	145		
	1208		87	
1316 (0.03)	1311	20		δ CNH
	1349		66	
1469 (0.23)	1444	123		δ CNH
	1487		290	ν C4-O8
1589 (1.00)	1558	349		ν C4-C5
	1602		519	ν C2-O2 + ν C4-C5
	1606	415		ν C5-C6 + ν N3-C4
	1630		442	ν C5-C6 + ν C2-N3
1800 (0.03)	1810	684		ν C2=O7

[a] scaled by a 0.96 scaling factor.

Table 3 : Measured (left column) and calculated vibrational spectra for protonated thymine. Normalized intensities of the experimental signal are given in parenthesis.

Wavenumber		Calculated intensities (km.mol^{-1})		Vibrational mode
Experimental	Calculated [a]	T1_hd	T2_ha	
1146 (0.15)	1103		129	δ COH or combined
	1121	66		δ COH/δ CCH modes
1200 (0.33)	1166		231	Combined
	1187	205		δ CNH/δ COH/δ CCH
	1200		146	modes
1368 (0.10)	1355		57	δ CNH
1474 (0.23)	1431	58		δ CNH+ δ CH_3
	1439	39		
	1472		265	ν C4-O8 + δ CH_3
1608 (1.00)	1599		485	ν C2-O7 + ν C4-C5
	1615	190		ν N3-C4+ ν C5-C6
	1628		330	ν C5-C6 + ν C2-N3
1800 (0.03)	1810	778		ν C2=O7

[a] scaled by a 0.96 scaling factor.

Table of content

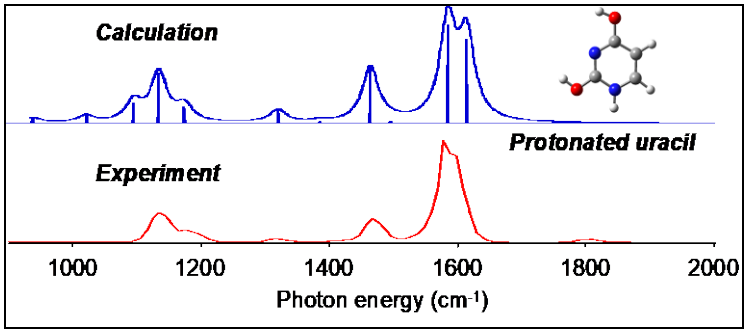

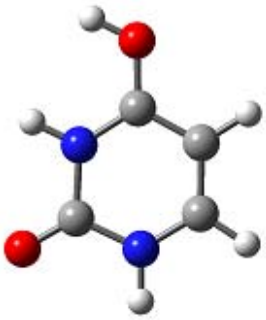

U1_hc +15.1

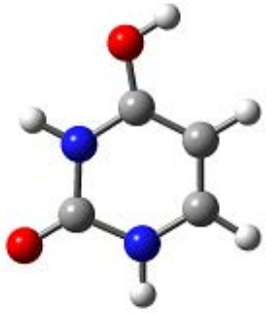

U1_hd +4.2

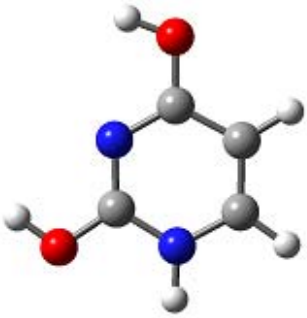

U2_ha 0

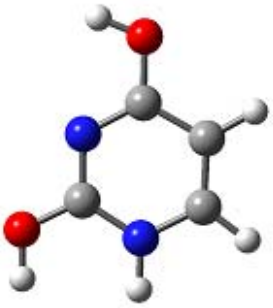

U2_hb +29.9

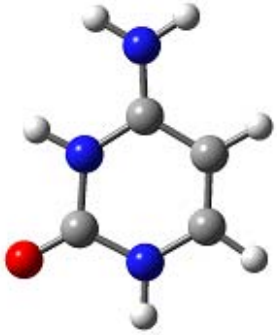

C1_hb +0.3

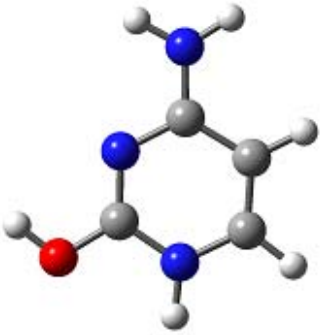

C1_hc 0

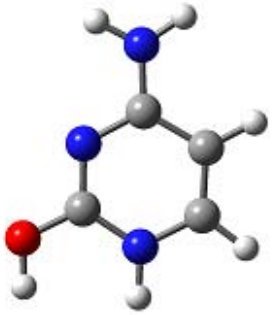

C1_hd 30.8

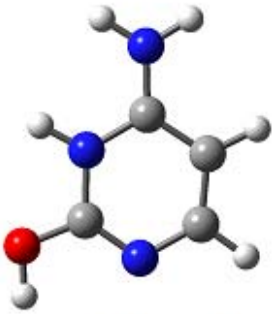

C4_hb +35.2

Figure 1

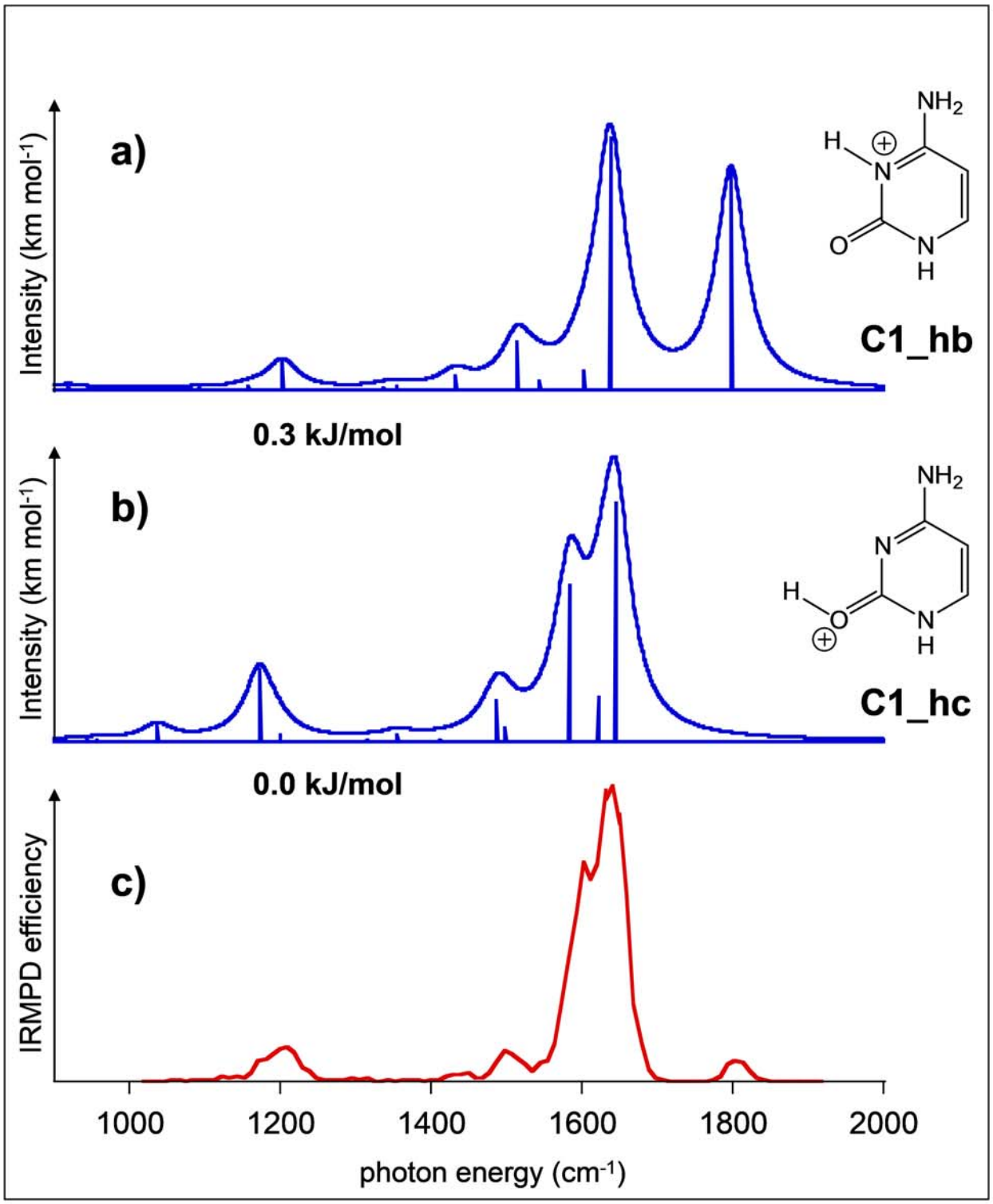
a)
Intensity (km mol-1)
NH2
H
N
O
N
H
C1_hb
0.3 kJ/mol
b)
Intensity (km mol-1)
NH2
N
H
O
N
H
C1_hc
0.0 kJ/mol
c)
IRMPD efficiency
1000
1200
1400
1600
1800
2000
photon energy (cm-1)

Figure 2

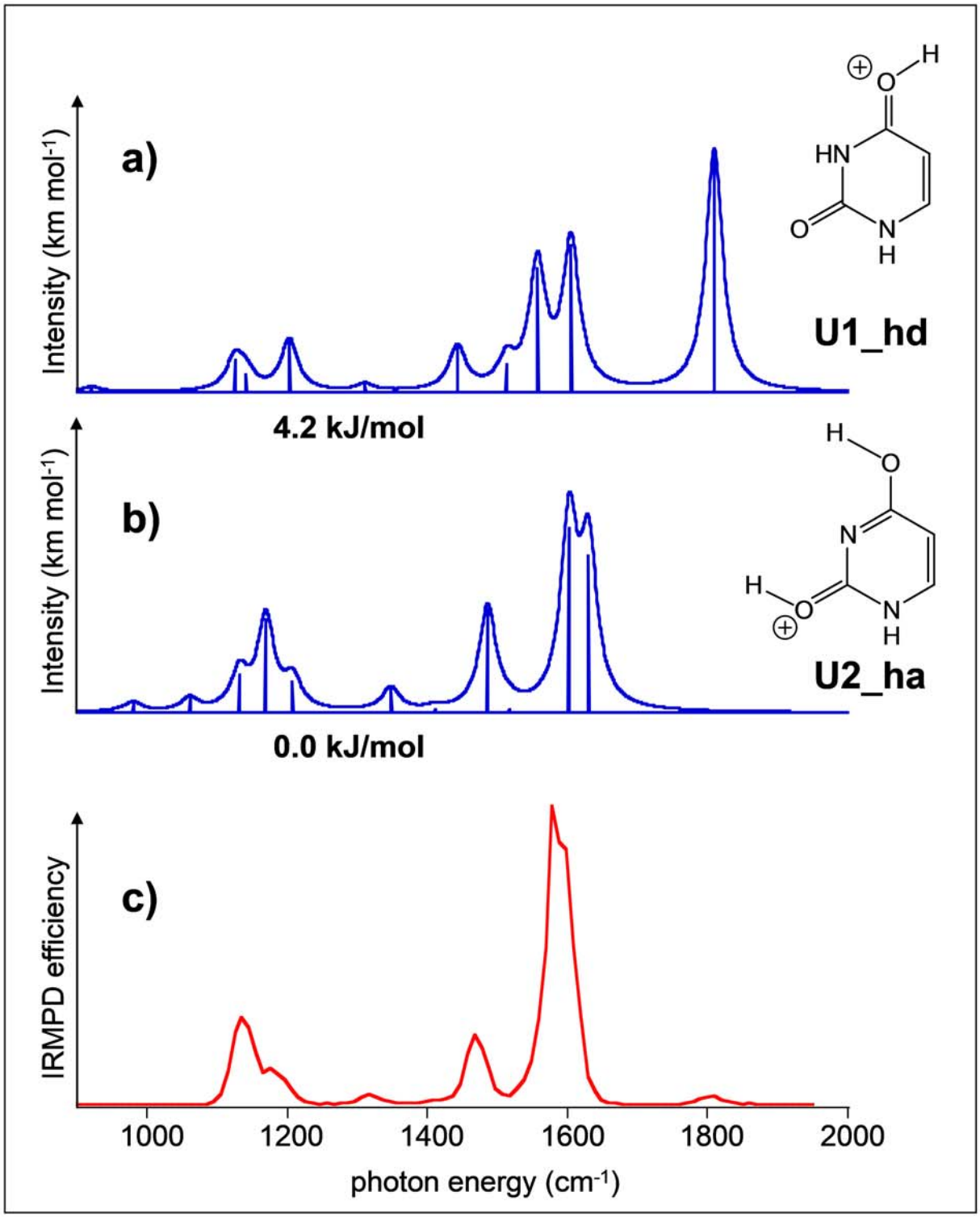
a)
Intensity (km mol-1)
U1_hd
4.2 kJ/mol
b)
Intensity (km mol-1)
U2_ha
0.0 kJ/mol
c)
IRMPD efficiency
1000
1200
1400
1600
1800
2000
photon energy (cm-1)

Figure 3

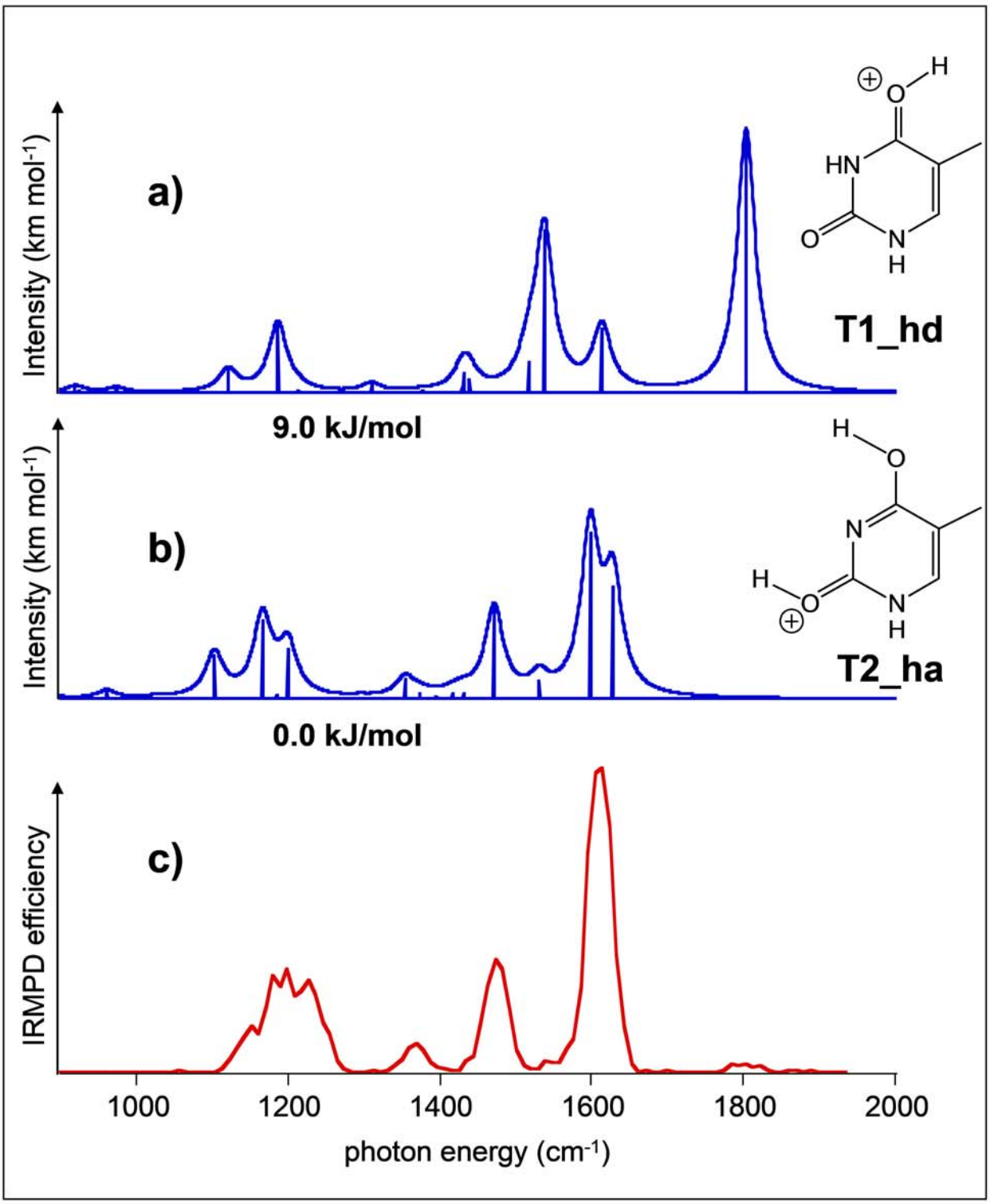
a)
Intensity (km mol-1)
T1_hd
9.0 kJ/mol
b)
Intensity (km mol-1)
T2_ha
0.0 kJ/mol
c)
IRMPD efficiency
1000
1200
1400
1600
1800
2000
photon energy (cm-1)

Figure 4

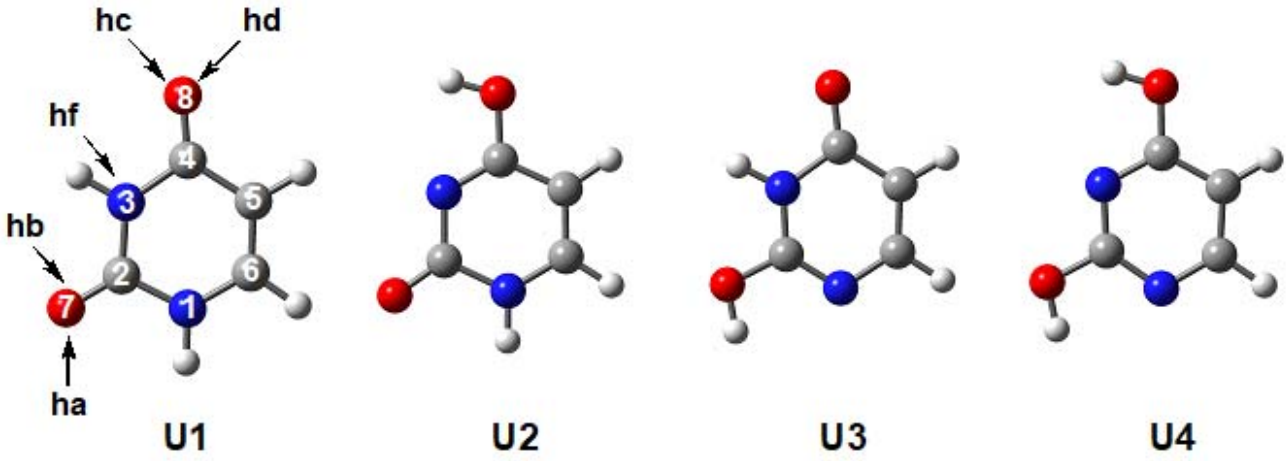

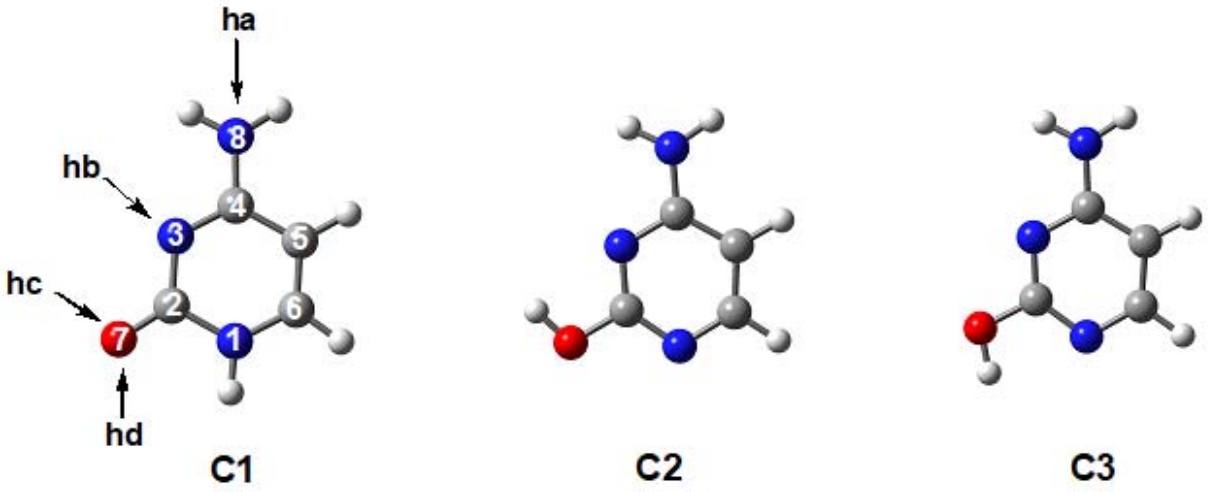

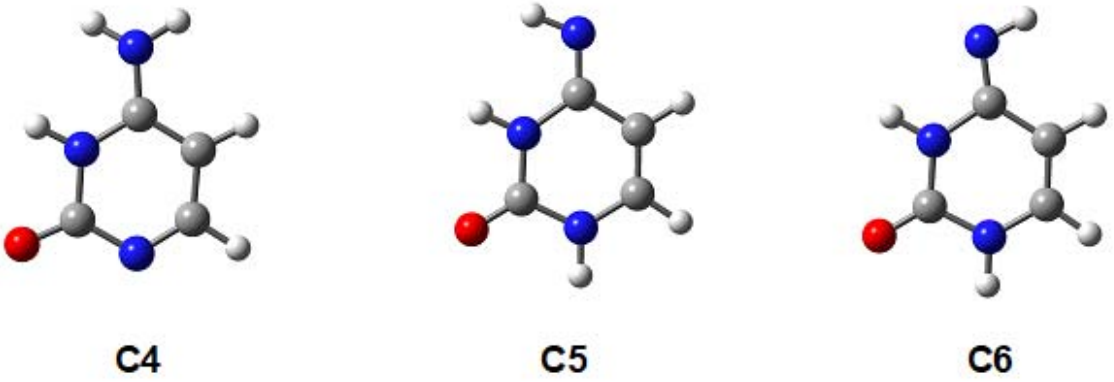

Scheme 1

Infrared spectra of protonated uracil, thymine and cytosine

Jean-Yves Salpin*, Sébastien Guillaumont and Jeanine Tortajada

Laboratoire d'Analyse et de Modélisation pour la Biologie et l'Environnement (LAMBE) Université d'Evry Val d'Esonne – CNRS – Bâtiment Maupertuis – Boulevard François Mitterrand – 91025 EVRY; FRANCE

Luke MacAleese, Joël Lemaire and Philippe Maître*
Laboratoire de Chimie Physique – Université Paris Sud Orsay – CNRS – 91405 ORSAY; FRANCE

Supporting information

1S. Total energy and ZPE (Hartree) of the various structures considered.

2S. Structure and relative energies (kJ/mol) at the B3LYP/6-311++G(3df,2p)//B3LYP/631++G(d,p) +ZPE level of the various structures envisaged

3S. B3LYP/6-311++G(3df,2p)//B3LYP/6-31++G(d,p) +ZPE potential energy surface associated with the gas-phase tautomerization of protonated uracil (relative energies are given in kJ/mol)

4S. B3LYP/6-311++G(3df,2p)//B3LYP/6-31++G(d,p) +ZPE potential energy surface associated with the tautomerization of gaseous or monohydrated uracil (values in kJ/mol)

5S. B3LYP/6-311++G(3df,2p)//B3LYP/6-31++G(d,p) +ZPE potential energy surface associated with the gas-phase tautomerization of protonated thymine (relative energies are given in kJ/mol)

6S. B3LYP/6-311++G(3df,2p)//B3LYP/6-31++G(d,p) +ZPE potential energy surface associated with the gas-phase tautomerization of protonated cytosine (relative energies are given in kJ/mol)

7S. B3LYP/6-311++G(3df,2p)//B3LYP/6-31++G(d,p) +ZPE potential energy surface associated with the gas-phase tautomerization of gaseous or monohydrated cytosine (relative energies are given in kJ/mol)

8S. B3LYP/6-31++G(d,p) vibrational spectrum of several protonated forms of uracil

9S. B3LYP/6-31++G(d,p) vibrational spectrum of several protonated forms of cytosine

1S. Total energy and ZPE (Hartree) of the various structures considered during this study.

1.1 Protonated uracil

Structure	B3LYP/6-31++G(d,p)		B3LYP//6-311++G(3df,2p)
	E	ZPE	E
U1_ha	-415.1676026	0.098782	-415.298051
U1_hb	-415.1698803	0.098913	-415.300077
U1_hc	-415.180879	0.099553	-415.310926
U1_hd	-415.1856461	0.099869	-415.315381
U1_he	-415.1534214	0.097965	-415.282048
U1_hf	-415.137452	0.098456	-415.266561
U1_hg	-415.130022	0.099066	-415.259156
U2_ha	-415.1878332	0.100034	-415.317153
U2_hb	-415.174425	0.099406	-415.305134
U2_hc	Equivalent to U1_hc		
U2_hd	-415.102894	0.097168	-415.232274
U3_ha	-415.175654	0.099502	-415.304853
U3_hb	-415.168528	0.098993	-415.298266
U3_hc	-415.083760	0.096487	-415.213009
U3_hd	Equivalent to U1_ha		
U3_he	-415.111224	0.097452	-415.240043
U3_hf	-415.147982	0.097680	-415.276173
U4_ha	Equivalent to U3_hb		
U4_hb	Equivalent to U2_hb		
U4_hc	-415.102903	0.097402	-415.231636
U4_hd	-415.102903	0.097658	-415.242841
U4_he	-415.114400	0.097993	-415.267720
TS1	-415.1183978	0.094698	-415.2475029
TS2	-415.1696071	0.098326	-415.2997245
TS3	-415.1618886	0.097872	-415.2918194
TS4	-415.1070548	0.093925	-415.2371398
TS5	-415.115812	0.094359	-415.2449748
TS6	-415.1716658	0.098211	-415.3011968
TS6	-415.1127285	0.094457	-415.2415937
TS8	-415.1630407	0.097915	-415.2907638

1.2 Neutral uracil

Structure	B3LYP/6-31++G(d,p)		B3LYP//6-311++G(3df,2p)
	E	ZPE	E
U1	-414.847479	0.086922	-414.975752
U2	-414.828468	0.086626	-414.957068
U3	-414.829803	0.086629	-414.957617
U4	-414.827109	0.086782	-414.954911
TS9	-414.777385	0.081690	-414.905236
TS10	-414.775617	0.081547	-414.902985
TS11	-414.768543	0.081660	-414.895925
TS12	-414.768355	0.081670	-414.895494

1.3 monohydrated uracil

Structure	B3LYP/6-31++G(d,p)		B3LYP//6-311++G(3df,2p)
	E	ZPE	E
U1_h2o	-491.296524	0.111672	-491.452255
U2_h2o	-491.282628	0.111738	-491.438125
TS13	-491.267306	0.105934	-491.420955

1.4 Protonated thymine

Structure	B3LYP/6-31++G(d,p)		B3LYP//6-311++G(3df,2p)
	E	ZPE	E
T1_ha	-454.496792	0.126436	-454.636349
T1_hb	-454.498749	0.126546	-454.638071
T1_hc	-454.506763	0.127225	-454.645619
T1_hd	-454.511056	0.127391	-454.649923
T1_he	-454.476695	0.126516	-454.614524
T1_hf	-454.463940	0.126264	-454.602097
T1_hg	-454.461119	0.126858	-454.599439
T2_ha	-454.515515	0.127741	-454.653699
T2_hb	-454.502401	0.127100	-454.641987
T2_hc	Equivalent to T1_hc		
T2_hd	-454.427638	0.124710	-454.565957
T3_ha	-454.501950	0.126969	-454.640278
T3_hb	-454.495491	0.126603	-454.634022
T3_hc	-454.412626	0.124166	-454.550981
T3_hd	Equivalent to T1_ha		
T3_he	-454.438450	0.125311	-454.576281
T3_hf	-454.470279	0.126122	-454.607666
T4_ha	Equivalent to T3_hb		
U4_hb	Equivalent to T2_hb		
T4_hc	-454.428956	0.124864	-454.566587
T4_hd	-454.441682	0.125277	-454.579062
T4_he	-454.461171	0.126501	-454.598784
TS14	-454.444527	0.121905	-454.582737
TS15	-454.498065	0.125993	-454.637066
TS16	-454.491586	0.125550	-454.630641
TS17	-454.436073	0.121473	-454.575174
TS18	-454.445246	0.122373	-454.583225
TS19	-454.497412	0.125791	-454.635829
TS20	-454.438156	0.121907	-454.576167
TS21	-454.490023	0.125411	-454.6281074

1.5 Neutral thymine

Structure	B3LYP/6-31++G(d,p)		B3LYP//6-311++G(3df,2p)
	E	ZPE	E
T1	-454.170374	0.114616	-454.307645
T2	-454.150049	0.114357	-454.287409
T3	-454.152990	0.114281	-454.289790
T4	-454.149196	0.114377	-454.285768

1.6 Protonated cytosine

Structure	B3LYP/6-31++G(d,p)		B3LYP//6-311++G(3df,2p)
	E	ZPE	E
C1_ha	-395.287746	0.112310	-395.405881
C1_hb	-395.339281	0.112463	-395.458804
C1_hc	-395.339819	0.112562	-395.459013
C1_hd	-395.325900	0.111839	-395.446570
C1_he	-395.288267	0.109912	-395.407787
C2_ha	-395.264113	0.110016	-395.382514
C2_hb	-395.285362	0.112221	-395.403444
C2_hc	-395.292919	0.110772	-395.411275
C3_ha	Equivalent to C2_ha		
C3_hb	-395.289980	0.112416	-395.407650
C3_hc	-395.293860	0.110784	-395.412333
C4_ha	-395.308413	0.110851	-395.429252
C4_hb	-395.325774	0.111876	-395.444912
C4_hc	-395.291200	0.110411	-395.410186
C4_hd	-395.250984	0.111243	-395.370180
C5_ha	-395.254859	0.111529	-395.374284
C5_hb	-395.255336	0.110820	-395.375035
C5_hc	-395.274711	0.110219	-395.312125
C5_hd	-395.285601	0.110762	-395.406706
C5_he	-295.385178	0.110739	-395.406321
C6_ha	-395.257782	0.111649	-395.377228
C6_hb	-395.264265	0.111528	-395.383054
C6_hc	-395.175475	0.110344	-395.394593
C6_hd	-395.293176	0.111295	-395.413639
C6_he	-395.290965	0.111096	-395.411713
TS22	-395.321623	0.110818	-395.441663
TS23	-395.274535	0.107383	-395.393317
TS24	-395.264168	0.1068547	-395.382918
TS25	-395.305826	0.110077	-395.426075

1.7 Neutral cytosine

Cytosine neutre			
C1	-394.963361	0.098164	-395.082423
C2	-394.961436	0.098545	-395.079615
C3	-394.962707	0.098572	-395.080823
C4	-394.952209	0.098030	-395.071194
C5	-394.957454	0.098906	-395.076688
C6	-394.960405	0.099117	-395.079563
TS26	-394.905156	0.093039	-395.022908
TS27	-394.947159	0.096967	-395.065472
TS28	-394.899773	0.093116	-395.017536
TS29	-394.894679	0.093102	-395.013308
TS30	-394.921926	0.095998	-395.041171

1.8 Monohydrated cytosine

Structure	B3LYP/6-31++G(d,p)		B3LYP//6-311++G(3df,2p)
	E	ZPE	E
C1_h2o	-471.416972	0.123288	-471.563244
C3_h2o	-471.413768	0.123680	-471.559373
TS31	-471.394801	0.117434	-471.538718

2S. Structure and relative energies (kJ/mol) at the B3LYP/6-311++G(3df,2p)//B3LYP/631++G(d,p) +ZPE level of the various structures envisaged

2.1 uracil

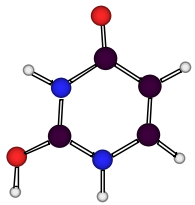

U1_ha 46.9

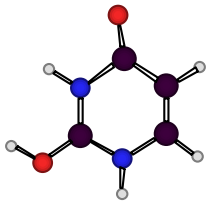

U1_hb 41.9

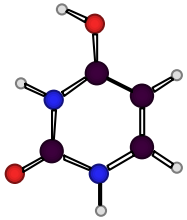

U1_hc 15.1

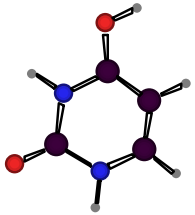

U1_hd 4.2

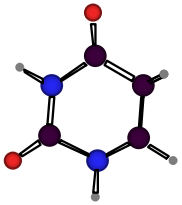

U1_he 86.7

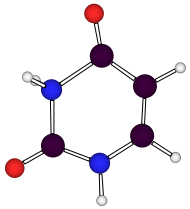

U1_hf 128.7

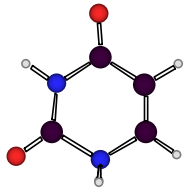

U1_hg 149.7

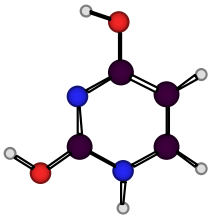

U2_ha 0

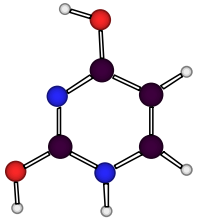

U2_hb 29.9

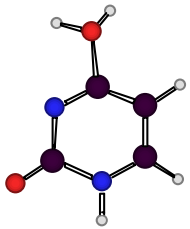

Ud_hd 215.3

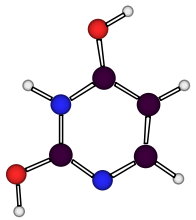

U3_ha 30.9

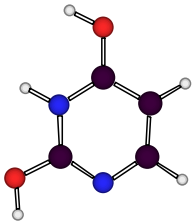

U3_hb 46.9

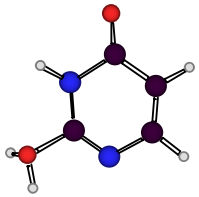

U3_hc 264.1

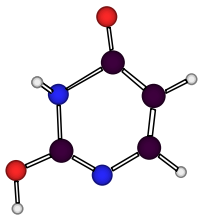

U3_he 195.7

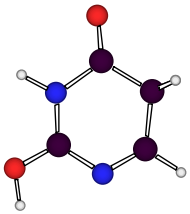

U3_hf 101.4

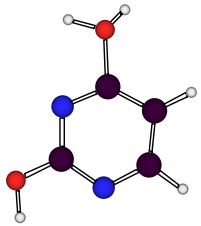

U4_hc 217.6

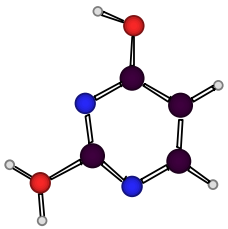

U4_hd 188.9

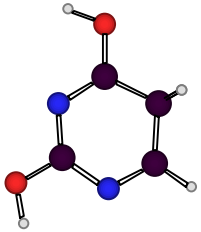

U4_he 124.4

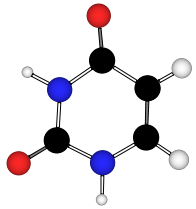

U1 0

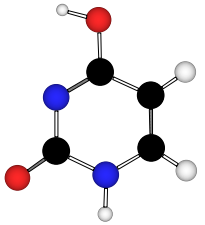

U2 48.3

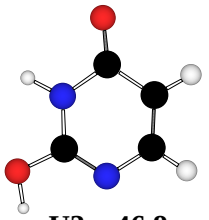

U3 46.8

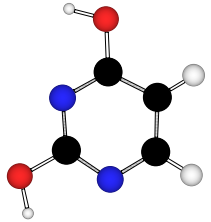

U4 54.4

2.2 Thymine

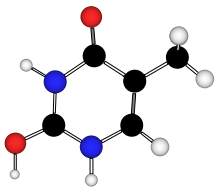

T1_ha 42.1

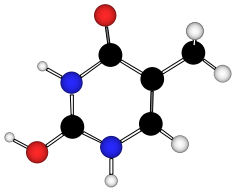

T1_hb 37.9

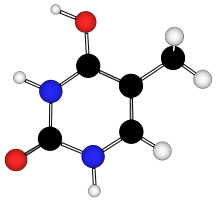

T1_hc 19.9

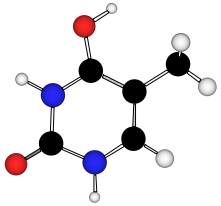

T1_hd 9.0

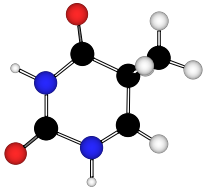

T1_he 99.6

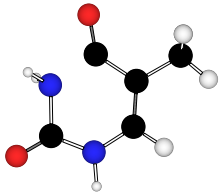

T1_hf 131.6

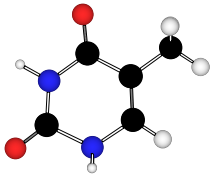

T1_hg 140.1

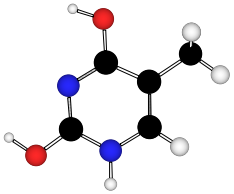

T2_ha 0

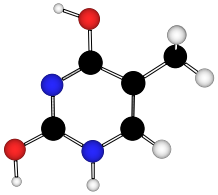

T2_hb 29.1

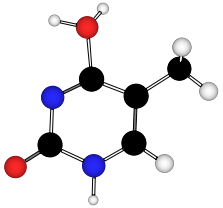

T2_hd 222.4

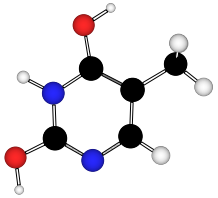

T3_ha 33.2

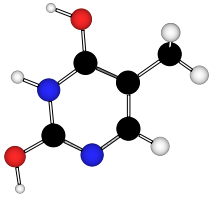

T3_hb 48.7

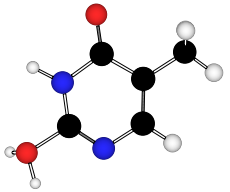

T3_hc 260.3

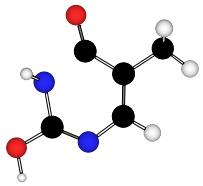

T3_he 196.9

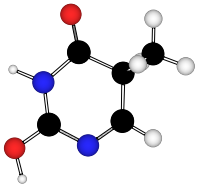

T3_hf 116.6

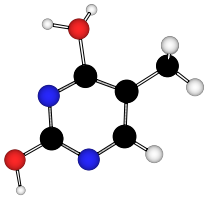

T4_hc 221.2

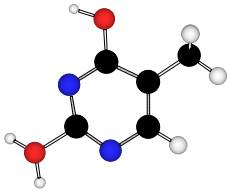

T4_hd 189.5

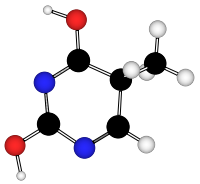

T4_he 140.9

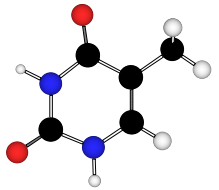

T1 0

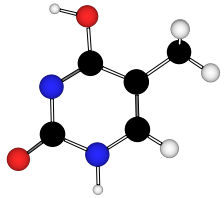

T2 52.4

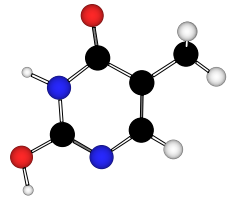

T3 46.0

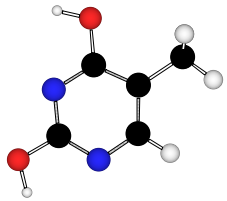

T4 56.8

2.3 Cytosine

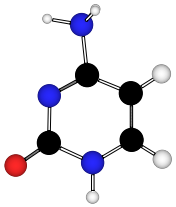

C1_ha 138.8

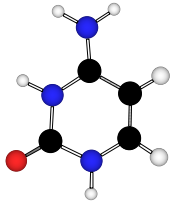

C1_hb 0.3

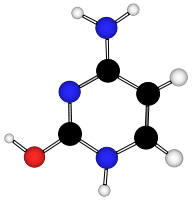

C1_hc 0

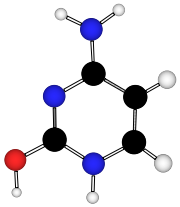

C1_hd 30.8

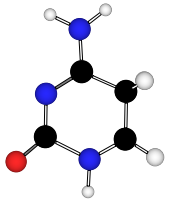

C1_he 127.5

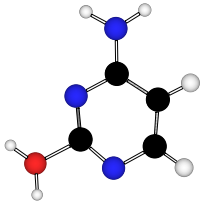

C2_ha 194.2

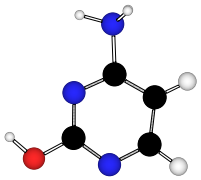

C2_hb 145.0

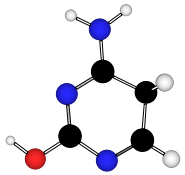

C2_hc 120.6

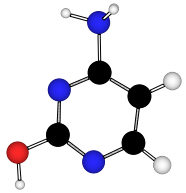

C3_hb 134.5

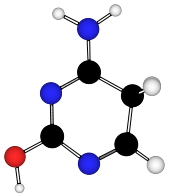

C3_hc 117.9

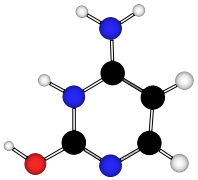

C4_ha 73.6

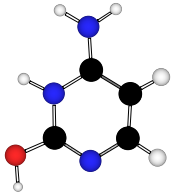

C4_hb 35.2

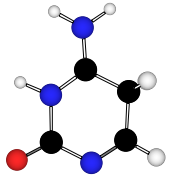

C4_hc 122.5

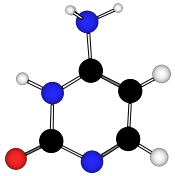

C4_hd 229.8

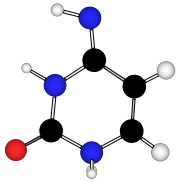

C5_ha 219.7

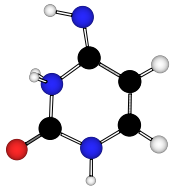

C5_hb 215.9

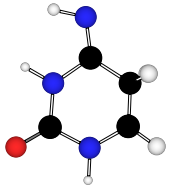

C5_hc 379.5

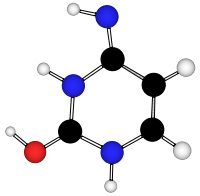

C5_hd 132.6

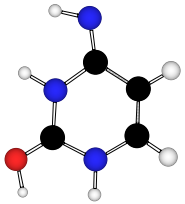

C5_he 133.6

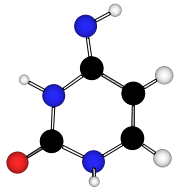

C6_ha 212.3

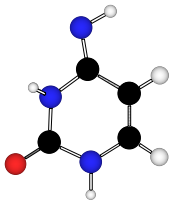

C6_hb 196.7

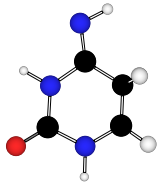

C6_hc 163.3

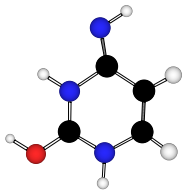

C6_hd 115.8

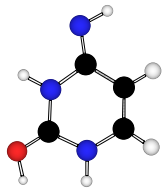

C6_he 120.3

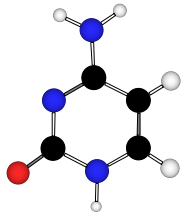

C1 0

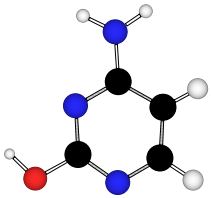

C2 8.4

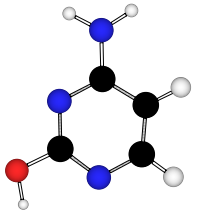

C3 5.3

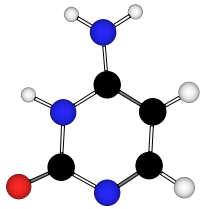

C4 29.1

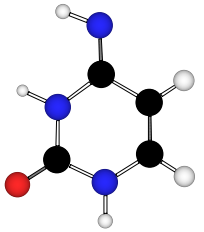

C5 17.0

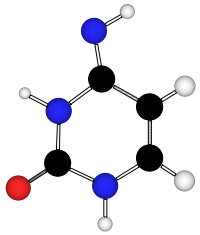

C6 10.0

3S. B3LYP/6-311++G(3df,2p)//B3LYP/6-31++G(d,p) +ZPE potential energy surface associated with the gas-phase tautomerization of protonated uracil (relative energies are given in kJ/mol)

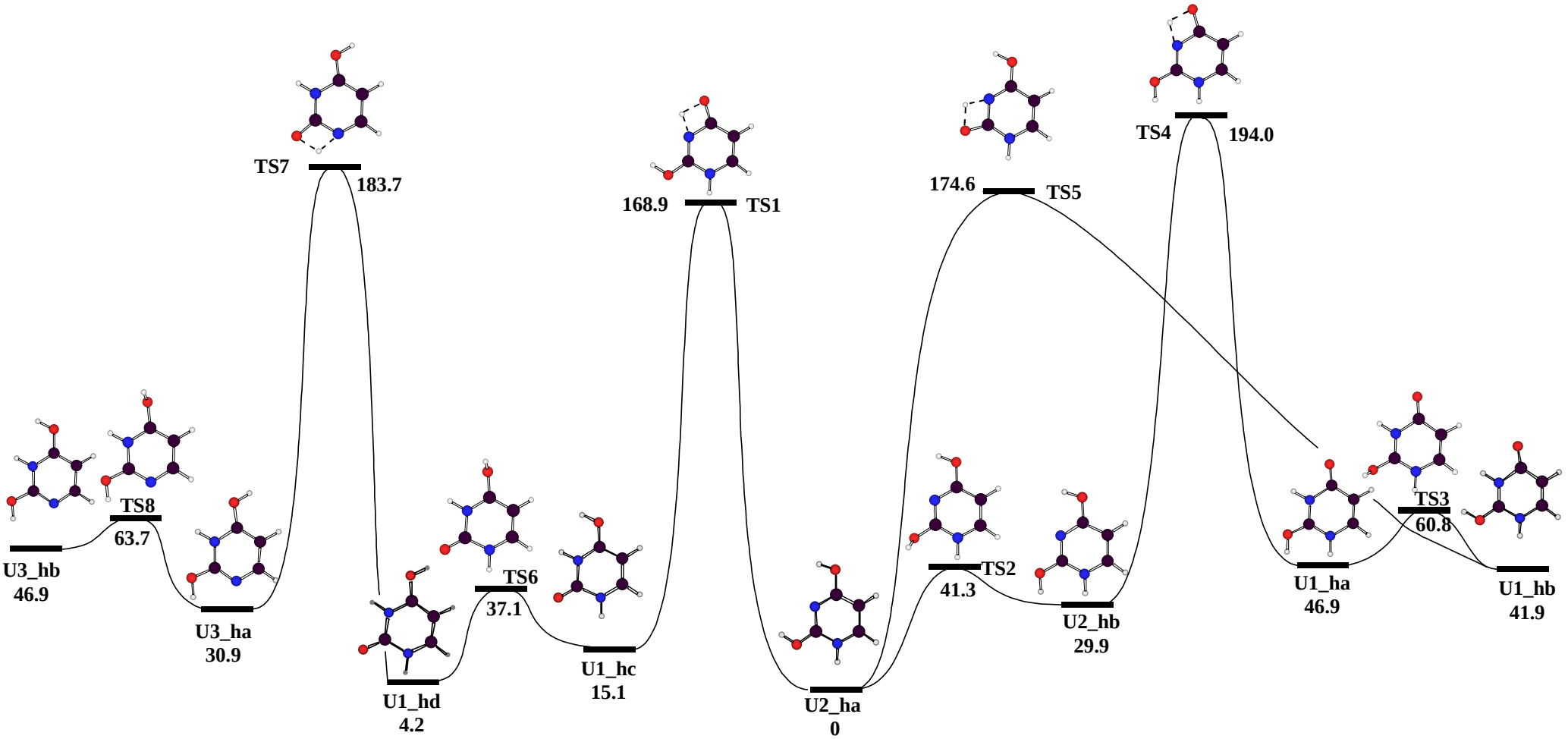

4S. B3LYP/6-311++G(3df,2p)//B3LYP/6-31++G(d,p) +ZPE potential energy surface associated with the tautomerization of gaseous or monohydrated uracil (values in kJ/mol)

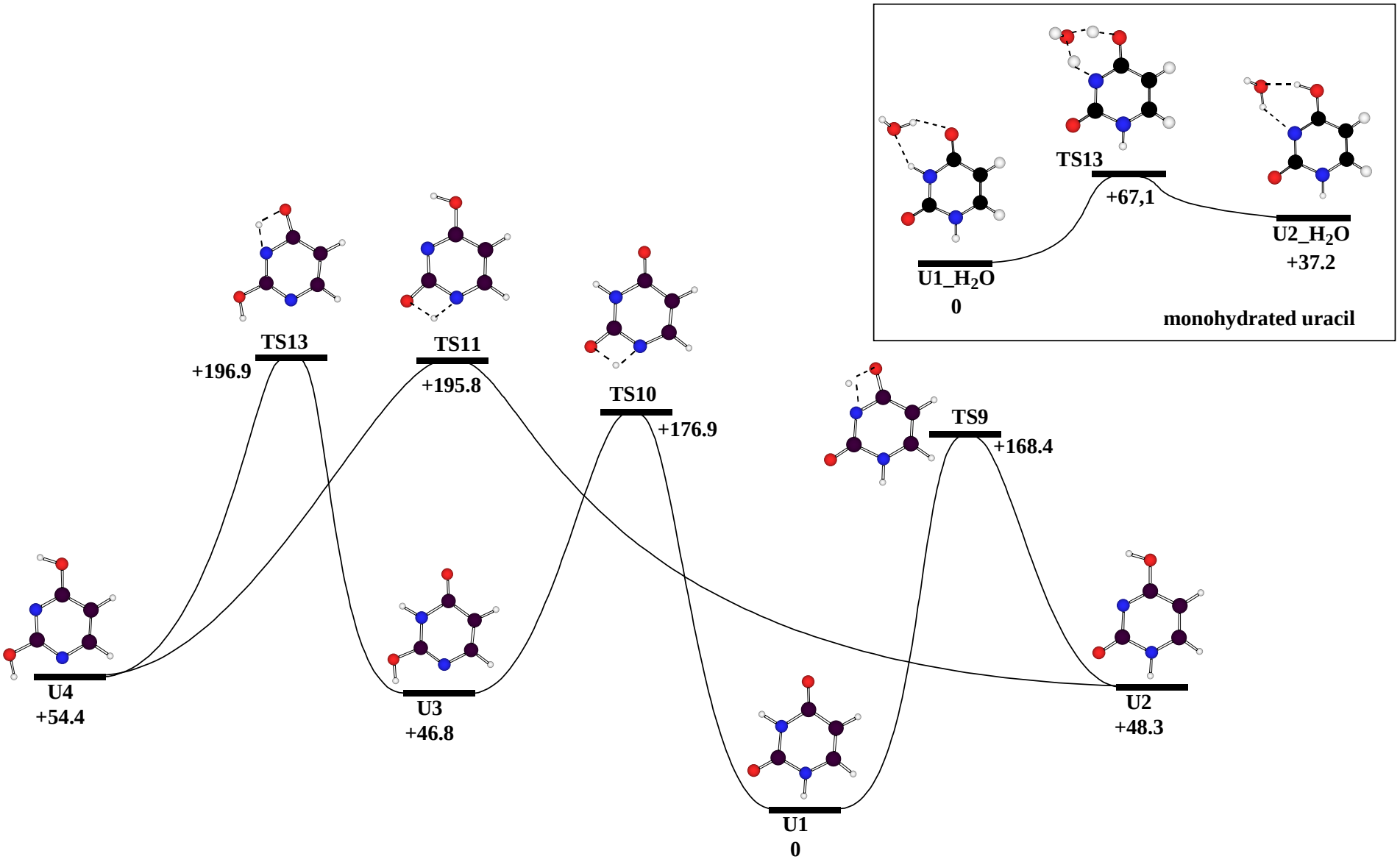

5S. B3LYP/6-311++G(3df,2p)//B3LYP/6-31++G(d,p) +ZPE potential energy surface associated with the gas-phase tautomerization of protonated thymine (relative energies are given in kJ/mol)

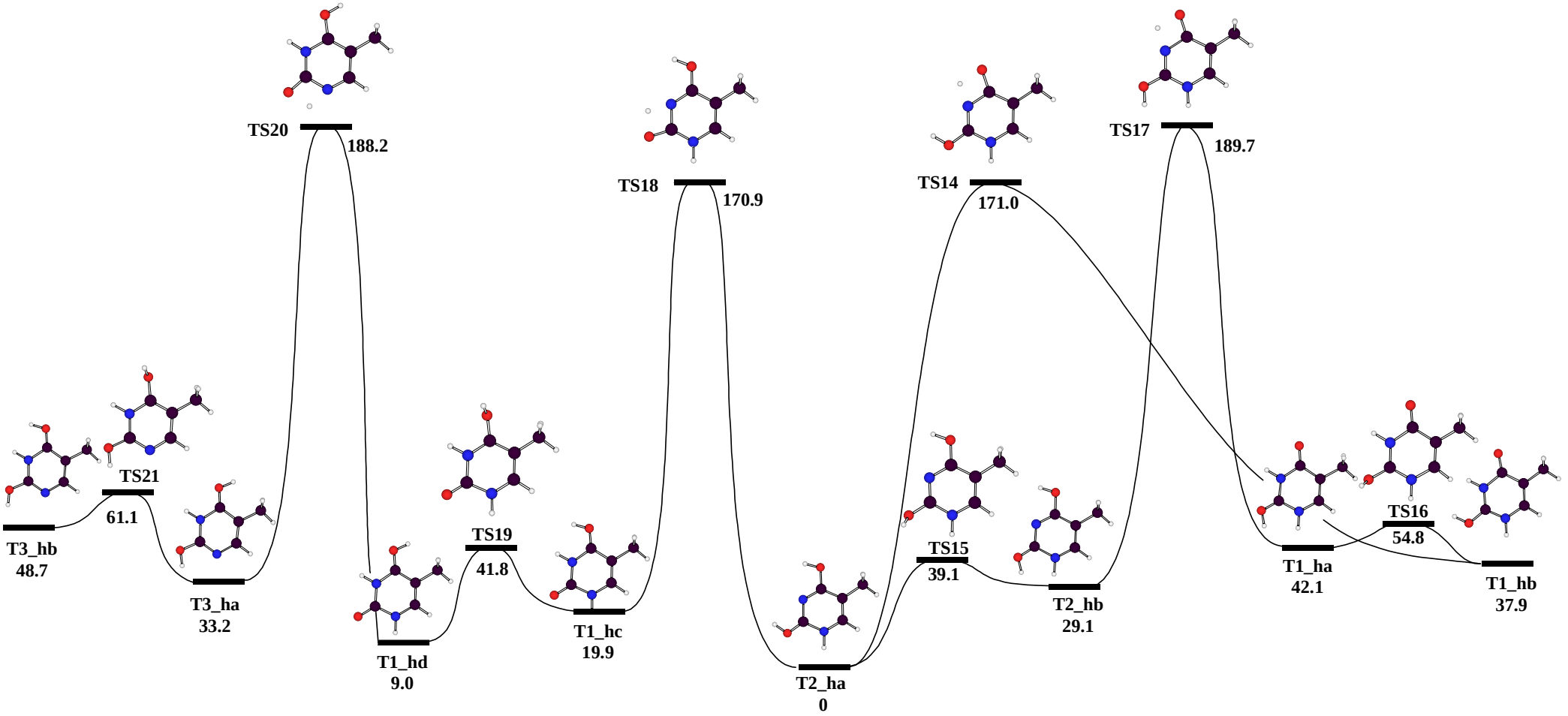

6S. B3LYP/6-311++G(3df,2p)//B3LYP/6-31++G(d,p) +ZPE potential energy surface associated with the gas-phase tautomerization of protonated cytosine (relative energies are given in kJ/mol)

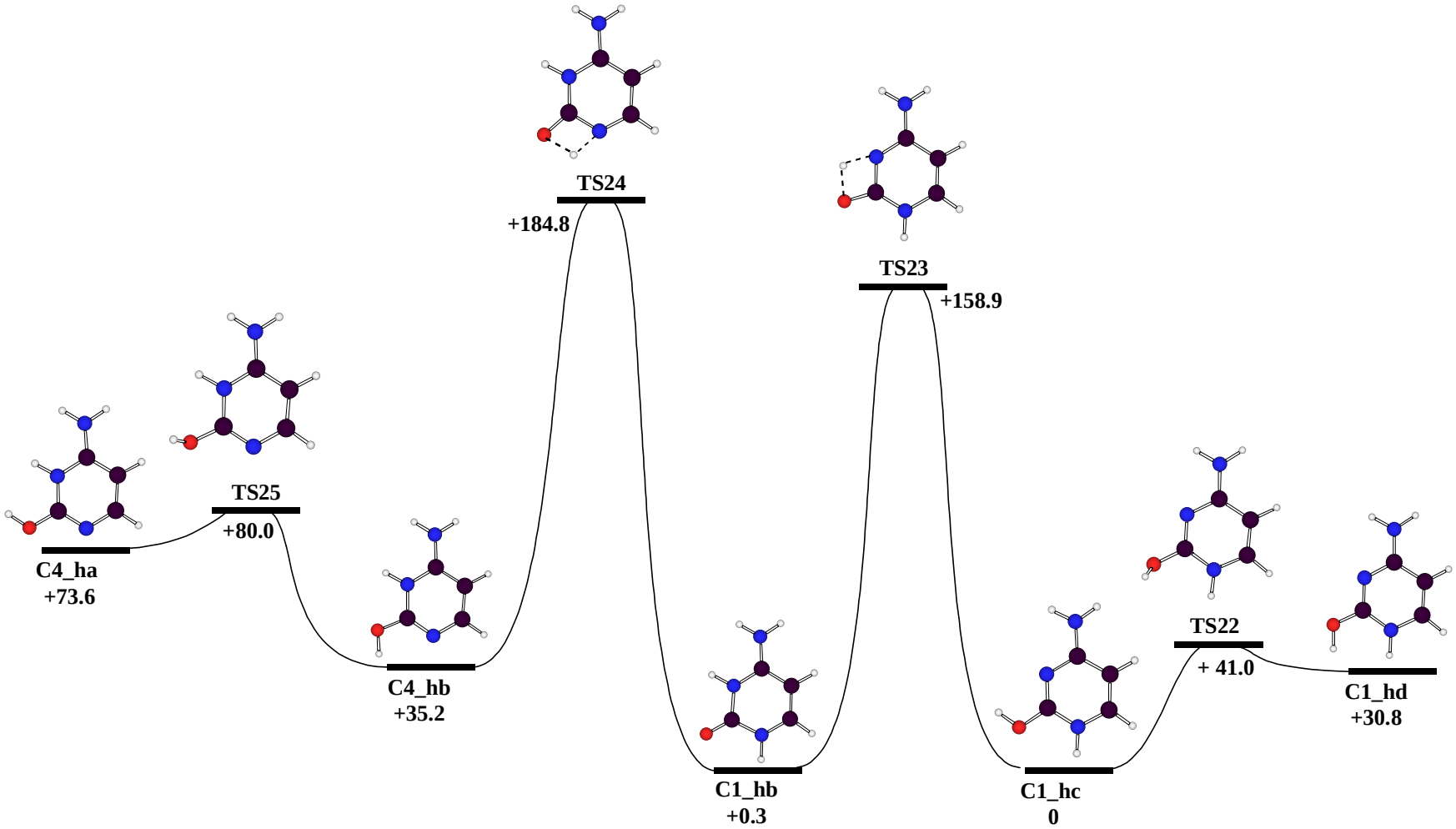

7S. B3LYP/6-311++G(3df,2p)//B3LYP/6-31++G(d,p) +ZPE potential energy surface associated with the gas-phase tautomerization of gaseous or monohydrated cytosine (relative energies are given in kJ/mol)

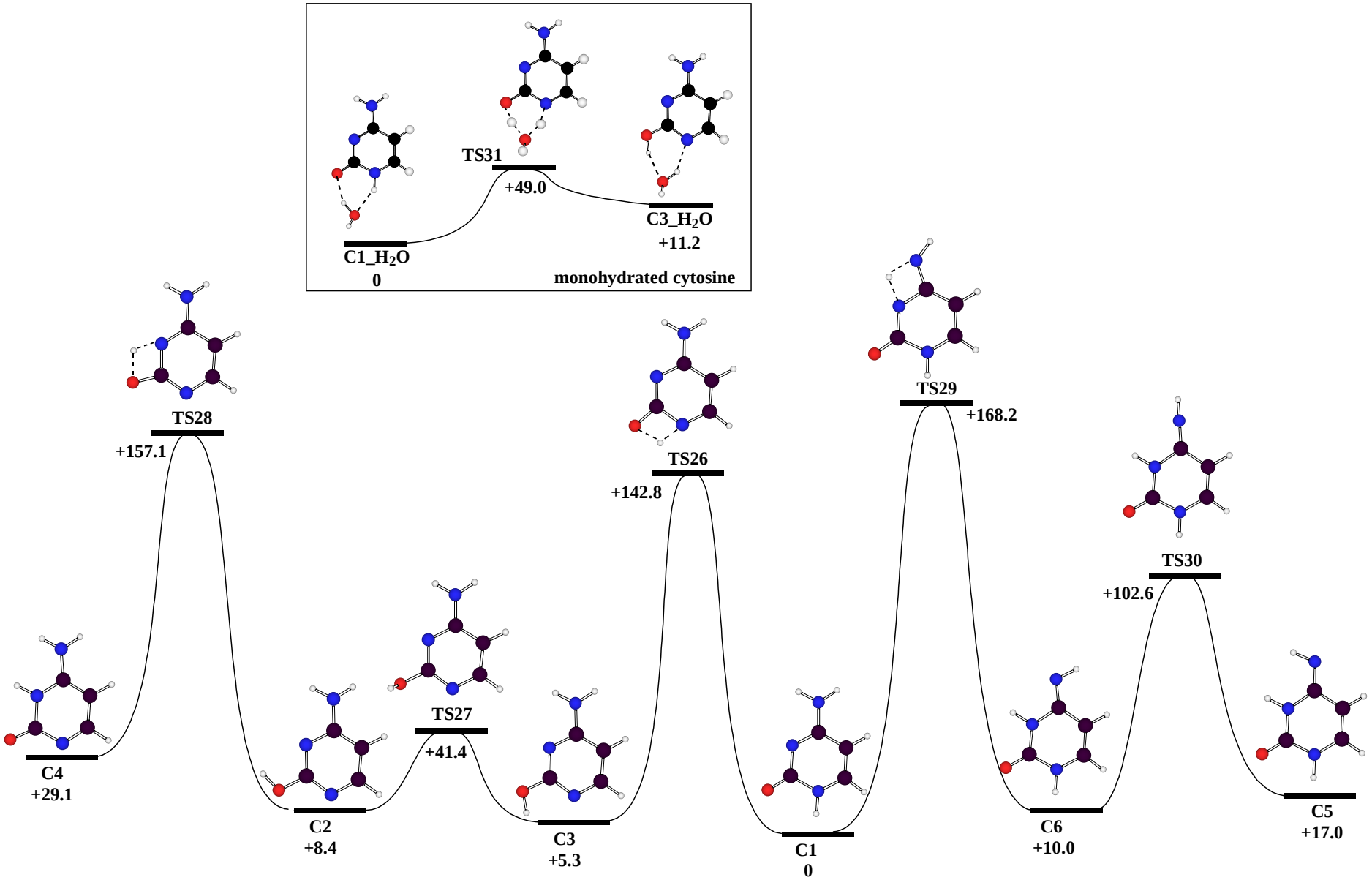

8S. B3LYP/6-31++G(d,p) vibrational spectrum of several protonated forms of uracil

Computed spectra are scaled by a factor of 0.96

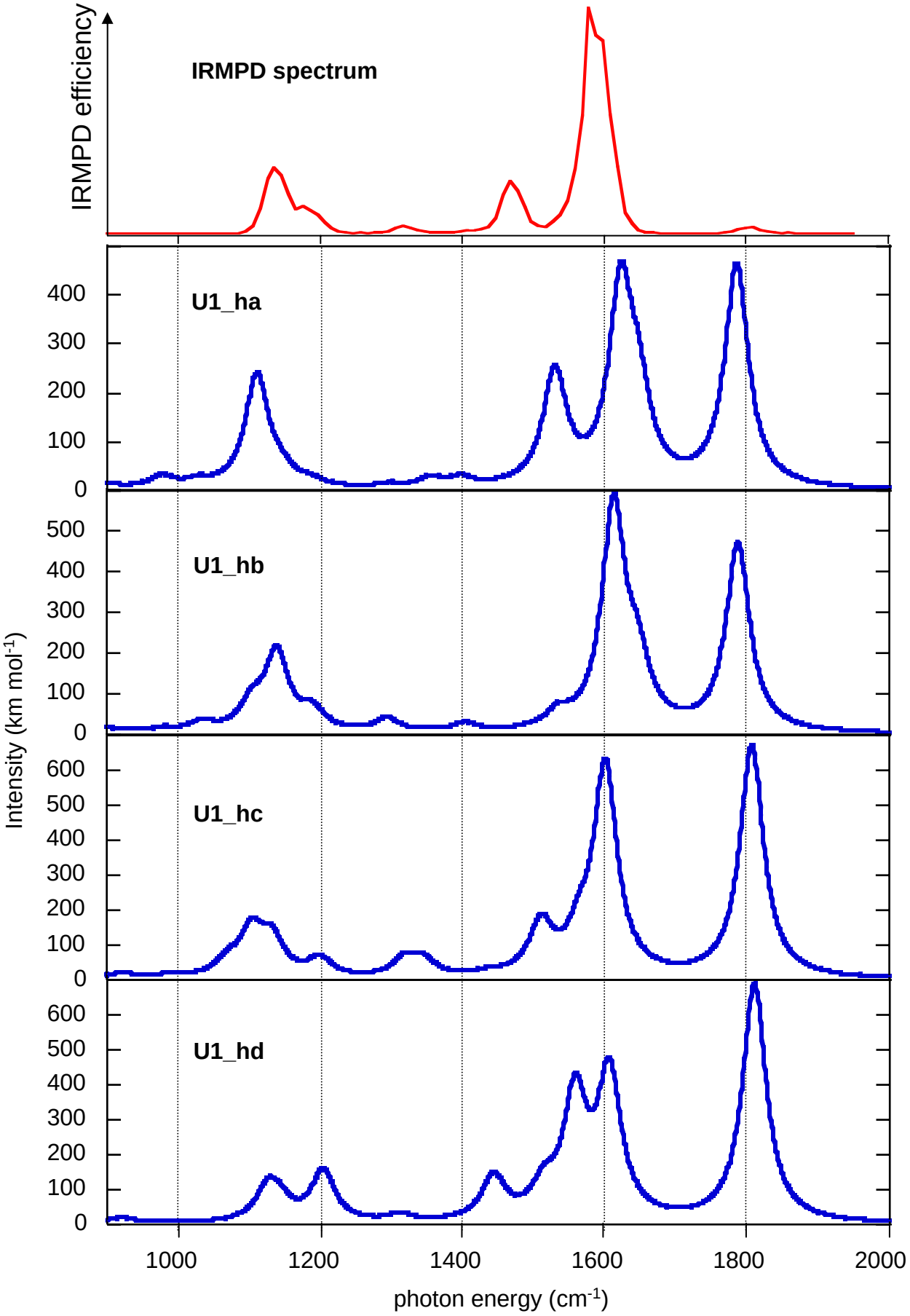

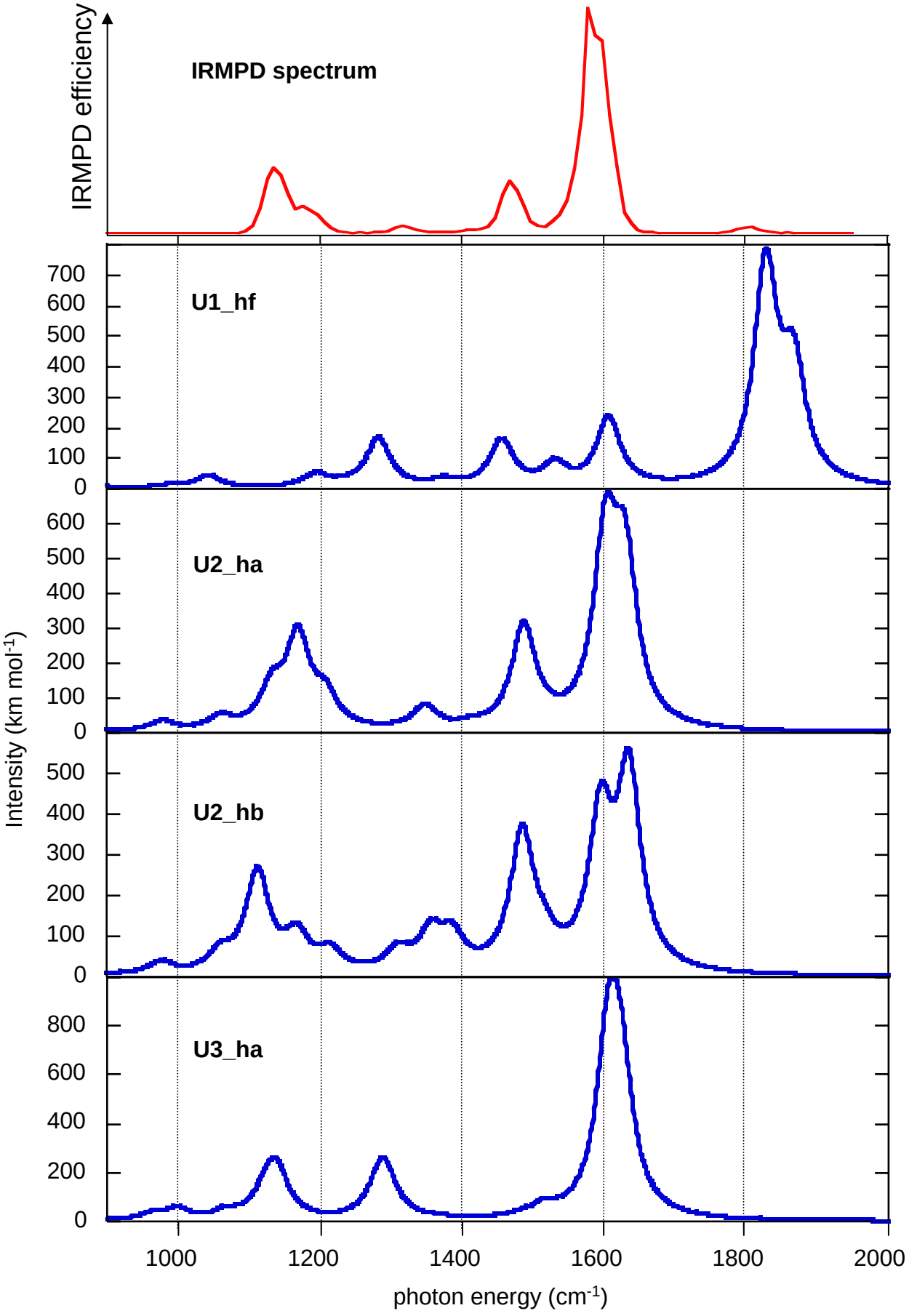
IRMPD efficiency
IRMPD spectrum
U1_hf
U2_ha
U2_hb
U3_ha
Intensity (km mol-1)
photon energy (cm-1)
0
100
200
300
400
500
600
700
800
1000
1200
1400
1600
1800
2000

9S. B3LYP/6-31++G(d,p) vibrational spectrum of the most stable protonated forms of cytosine

Computed spectra are scaled by a factor of 0.96

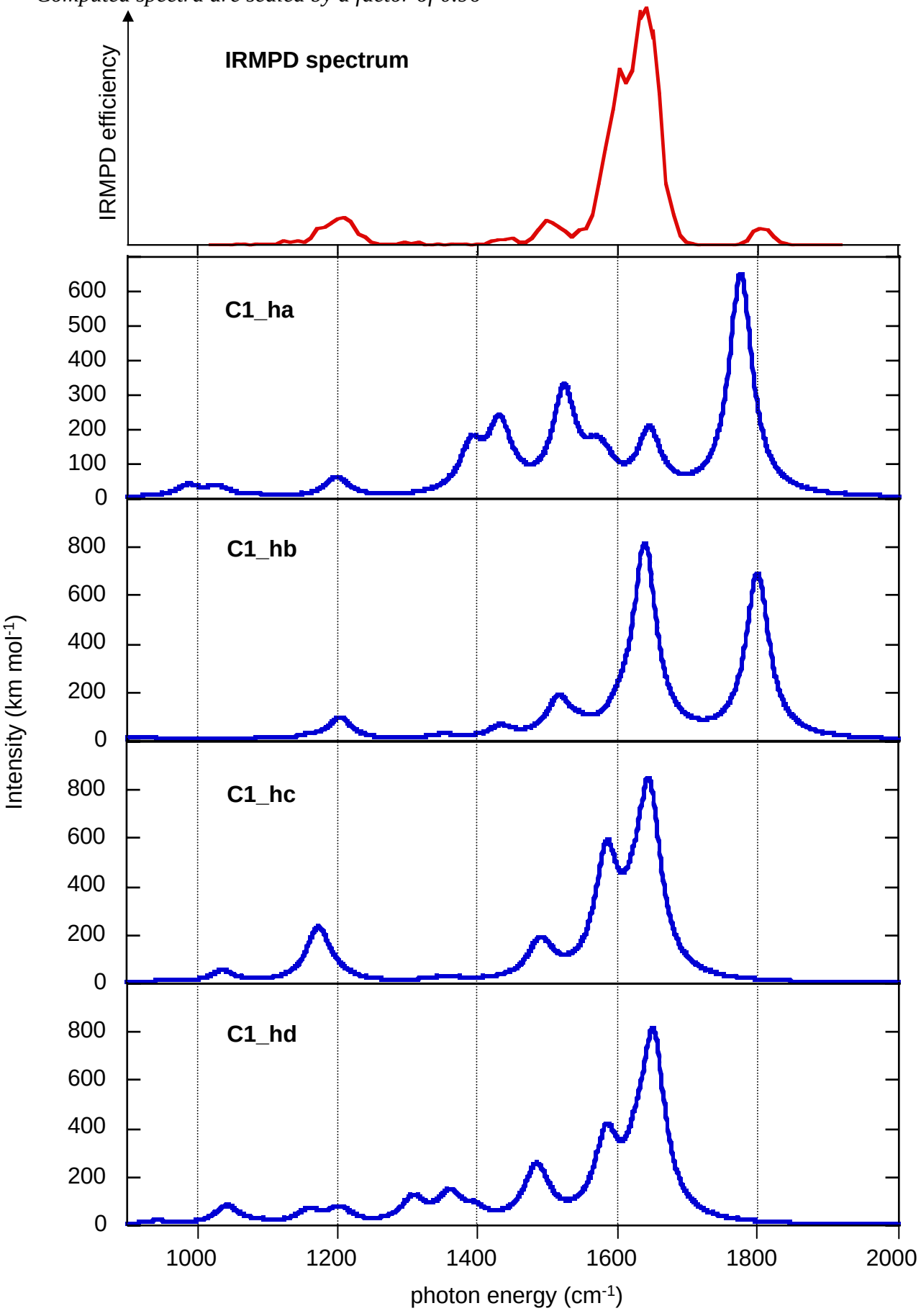

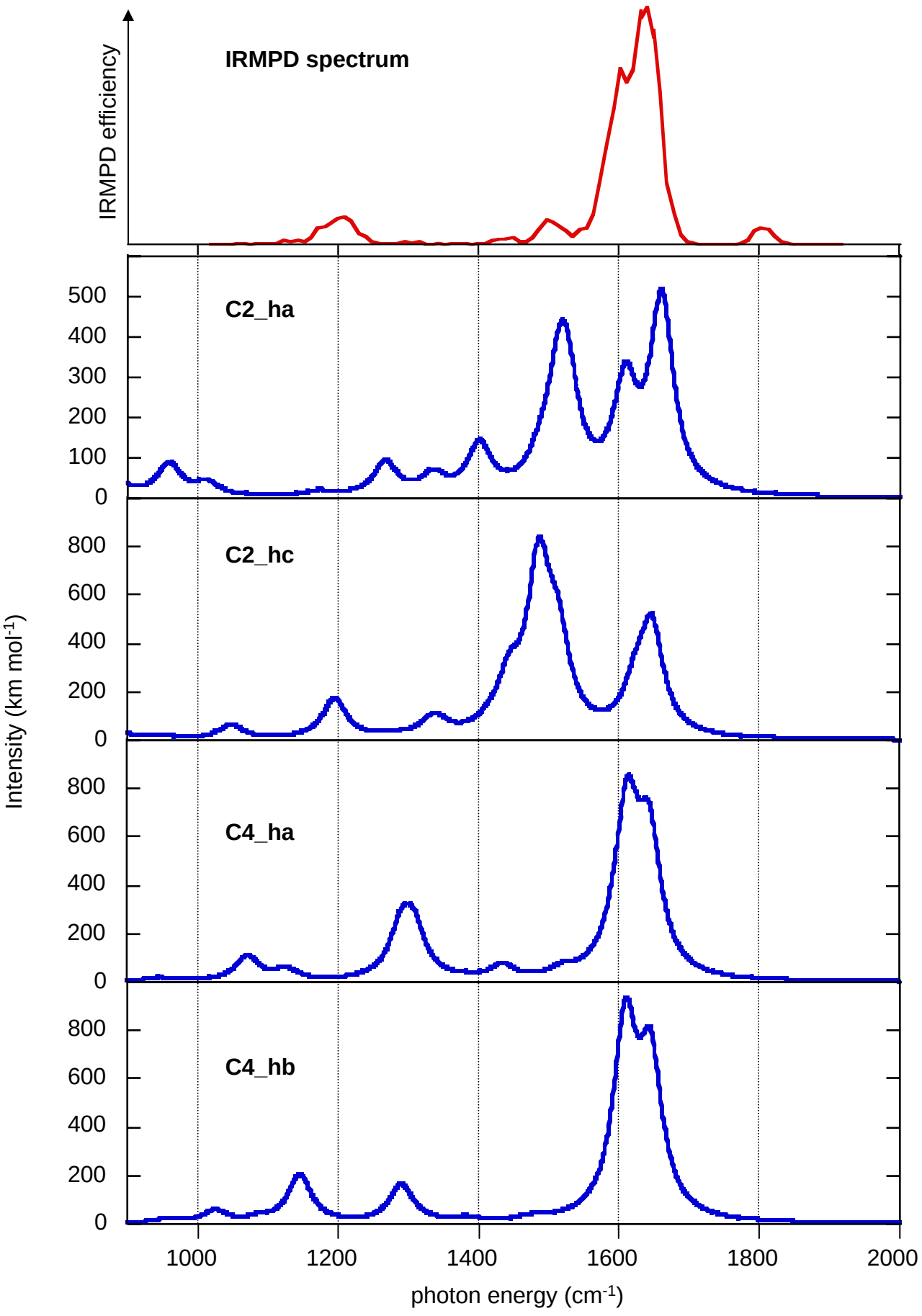
IRMPD spectrum
IRMPD efficiency
C2_ha
C2_hc
C4_ha
C4_hb
Intensity (km mol-1)
photon energy (cm-1)
0
100
200
300
400
500
600
800
1000
1200
1400
1600
1800
2000